Cyanido-Bridged Fe(III)−Mn(III) Heterobimetallic Materials Built From Mn(III) Schiff Base Complexes and Di- or Tri-Cyanido Fe(III) Precursors

Tapas Senapati,[†,‡] Céline Pichon,*[,†,‡] Rodica Ababei,[†,‡,§,⊥] Corine Mathonière,[§,⊥] and Rodolphe Clérac*[,†,‡]

[†]CNRS, CRPP, UPR 8641, Centre de Recherche Paul Pascal, Equipe "Matériaux Moléculaires Magnétiques", 115 avenue du Dr. Albert Schweitzer, F-33600 Pessac, France

[‡]Univ. Bordeaux, CRPP, UPR 8641, F-33600 Pessac, France

[§]CNRS, ICMCB, UPR 9048, Institut de Chimie de la Matière Condensée de Bordeaux, 87 Avenue du Dr. Albert Schweitzer, F-33608 Pessac, France

[⊥]Univ. Bordeaux, ICMCB, UPR 9048, F-33608 Pessac, France

ⓢ *Supporting Information*

ABSTRACT: The reaction of $[Fe^{III}L(CN)_3]^-$ (L being bpca = bis(2-pyridylcarbonyl)amidate, pcq = 8-(pyridine-2-carboxamido)quinoline) or $[Fe^{III}(bpb)(CN)_2]^-$ (bpb = 1,2-bis(pyridine-2-carboxamido)benzenate) ferric complexes with Mn^{III} salen type complexes afforded seven new bimetallic cyanido-bridged Mn(III)−Fe(III) systems: $[Fe(pcq)(CN)_3Mn(saltmen)-(CH_3OH)]\cdot CH_3OH$ (**1**), $[Fe(bpca)(CN)_3Mn(3-MeO-salen)-(OH_2)]\cdot CH_3OH\cdot H_2O$ (**2**), $[Fe(bpca)(CN)_3Mn(salpen)]$ (**3**), $[Fe(bpca)-(CN)_3Mn(saltmen)]$ (**4**), $[Fe(bpca)(CN)_3Mn(5-Me-saltmen)]\cdot 2CHCl_3$ (**5**), $[Fe(pcq)(CN)_3Mn(5-Me-saltmen)]\cdot 2CH_3OH\cdot 0.75H_2O$ (**6**), and $[Fe(bpb)-(CN)_2Mn(saltmen)]\cdot 2CH_3OH$ (**7**) (with saltmen^{2-} = N,N'-(1,1,2,2-tetramethylethylene)bis(salicylideneiminato) dianion, salpen^{2-} = N,N'-propylenebis(salicylideneiminato) dianion, salen^{2-} = N,N'-ethylenebis-(salicylideneiminato) dianion). Single crystal X-ray diffraction studies were carried out for all these compounds indicating that compounds **1** and **2** are discrete dinuclear [Fe(III)−CN−Mn(III)] complexes while systems **3**−**7** are heterometallic chains with {−NC−Fe(III)−CN−Mn(III)} repeating units. These chains are connected through π−π and short contact interactions to form extended supramolecular networks. Investigation of the magnetic properties revealed the occurrence of antiferromagnetic Mn(III)···Fe(III) interactions in **1**−**4** while ferromagnetic Mn(III)···Fe(III) interactions were detected in **5**−**7**. The nature of these Mn(III)···Fe(III) magnetic interactions mediated by a CN bridge appeared to be dependent on the Schiff base substituent. The packing is also strongly affected by the nature of the substituent and the presence of solvent molecules, resulting in additional antiferromagnetic interdinuclear/interchain interactions. Thus the crystal packing and the supramolecular interactions induce different magnetic properties for these systems. The dinuclear complexes **1** and **2**, which possess a paramagnetic $S_T = 3/2$ ground state, interact antiferromagnetically in their crystal packing. At high temperature, the complexes **3**−**7** exhibit a one-dimensional magnetic behavior, but at low temperature their magnetic properties are modulated by the supramolecular arrangement: a three-dimensional antiferromagnetic order with a metamagnetic behavior is observed for **3**, **4**, and **7**, and Single-Chain Magnet properties are detected for **5** and **6**.
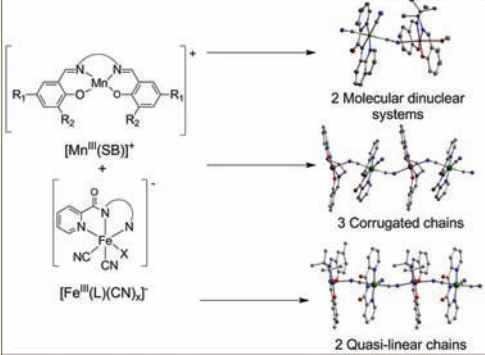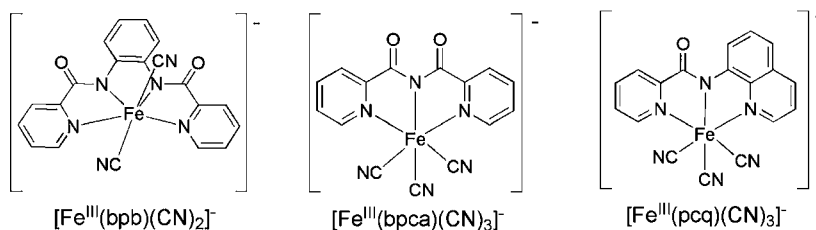
INTRODUCTION

In the past three decades, molecular magnetic materials have attracted extensive interest in various scientific fields including chemistry, physics, materials science, and catalysis.[1] Cyanido-metallates are the most extensively used metalloligands with which to prepare molecule-based magnetic materials with diverse architectures and properties capitalizing on the coordination ability of the CN⁻ group to bridge two metal ions.[2] The cyanido ligand is also well-known to be a remarkable magnetic linker that mediates efficient ferro- or antiferro-magnetic exchange interactions between paramagnetic centers

depending on the structural parameters.[3] Rational design of materials can be achieved following a building-block approach with the premeditated association of various complexes and capped cyanidometallates $[M(L)_x(CN)_y]^{z-}$ (L = tridentate or tetradentate ligand) that promote compounds with low dimensionality. Different heterometallic molecular arrangements,[4] in particular cubes[5] and squares[6] but also one and two-dimensional networks,[7] were reported following this
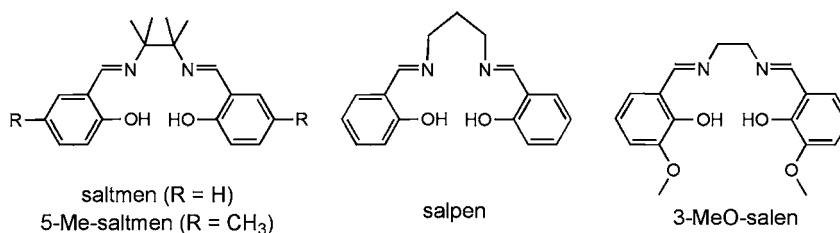
Scheme 1

[Fe^{III}(bpb)(CN)$_2$]$^-$ [Fe^{III}(bpca)(CN)$_3$]$^-$ [Fe^{III}(pcq)(CN)$_3$]$^-$

Scheme 2

saltmen (R = H)
5-Me-saltmen (R = CH$_3$)   salpen   3-MeO-salen

synthetic strategy. The isolation of such molecular systems is of interest to establish magneto-structural correlations to elucidate magnetic pathways through cyanido bridges. Furthermore, selection of appropriate building blocks exhibiting targeted chemical (number of cyanido groups, steric hindrance of the ligand, etc.) and physical properties (local anisotropy, spin state, etc.) afforded a family of original materials with controlled structures and properties. Following this synthetic strategy, remarkable magnetic properties such as Single-Molecule Magnet (SMM)[2p,5b,d,e,6e,p,8] and Single-Chain Magnet (SCM)[9] behaviors have been obtained. SMMs and SCMs are characterized by the existence of slow relaxation of their magnetization at the molecular level, an attractive property for fundamental sciences (for example, to explore quantum effects such as magnetization tunneling or quantum phase interferences) but also for their potential applications in molecular magnetic information storage or quantum calculation.[10]

These fascinating SMM and SCM systems can be obtained following a rationalized approach combining anisotropic units linked via paramagnetic bridges inducing strong magnetic interactions. For example, it has been shown by Long et al. that SCMs can be synthesized with mononuclear anisotropic components in an equimolar ratio, as in the [(DMF)$_4$MReCl$_4$(CN)$_2$] (M = Mn, Fe, Co, Ni) family of compounds.[9f] On the other hand, Mn(III) Schiff base complexes are valuable anisotropic sources to design SCMs as demonstrated with the synthesis of [Mn$_2$(5-MeO-saltmen)$_2$Fe(CN)$_6$]$^-$ (saltmen^{2-} = N,N'-(1,1,2,2-tetramethylethylene)bis(salicylideneiminato) dianion)[11] or [Mn^{III}(5-TMAM-salen)M^{III}(CN)$_6$]·4H$_2$O (5-TMAM-salen^{2-} = N,N'-(ethylene)bis(5-trimethylammoniomethyl)-salicylideneiminato dianion, M^{III} = Co^{III}, Fe^{III}, Mn^{III}, Cr^{III})[12] by Miyasaka and co-workers following a step by step rational synthetic strategy based on the association of Mn(III)/salen precursors with hexacyanidoferrate. In addition to their intrinsic magnetic anisotropy (giving rise to SMM behavior in dimeric entities[13]) and their structural versatility, these Schiff base complexes are very appealing building blocks to design one-dimensional (1D) systems because their axial positions are occupied by labile anions or solvent molecules easily substitutable by nucleophilic nitrogen atoms such as terminal cyanido groups. Among all the possible cyanido-based

complexes that could bridge these Mn^{III}/salen units, trans-cyanidometallate complexes capped with tri- or tetra-dentate ligand appear to be more appropriate linkers than hexacyano-metallates to promote molecular or 1D systems with potential SMM or SCM properties, since they possess a limited number of coordinating donor sites. For example, [Fe^{III}L^1(CN)$_3$]$^-$,[14] and [Fe^{III}L^2(CN)$_2$]$^-$,[6h,15] (L^1 and L^2 being tridentate or tetradentate N-donor ligands, respectively) were extensively used as precursors in the presence of Schiff base complexes in 1:1 stoichiometry.[16] The tridentate nitrogen donor ligand L^1 can be coordinated to the Fe(III) metal ion in a meridional (mer) or facial (fac) conformation, inducing a large family of precursors that have been synthesized with diverse ligands such as (i) hydrotris(pyrazolyl)borate (Tp), hydrotris-(3,5-dime-thylpyrazol-1-yl)borate (Tp*), tetra(pyrazol-1-yl)borate (pzTp), and 1,3,5-triaminocyclohexane (tach) for fac-Fe precursors[5a,14b,17] and (ii) bis(2-pyridylcarbonyl)amide anion (bpca), 8-(pyridine-2-carboxamido)quinoline anion (pcq), 8-(pyrazine-2-carboxamido)quinoline anion (pzcq), 8-(5-methylpyrazine-2-carboxamido)quinoline anion (mpzcq), and 8-(2-quinolinecarboxamido)quinoline anion (qcq) for mer-Fe building blocks.[18] In our quest to obtain new SMM or SCM systems, tricyanido mer-Fe(III) complexes attracted our interest because of the T shaped arrangement of their CN ligands, which could stabilize linear complexes or chains while the fac-Fe(III) would unlikely lead to such linear systems. Therefore, the reactivity of two different tricyanidometallate precursors, [Fe(bpca)(CN)$_3$]$^-$ and [Fe(pcq)(CN)$_3$]$^-$ anions and one dicyanidometallate building block [Fe(bpb)(CN)$_2$]$^-$ (bpb = 1,2-bis(pyridine-2-carboxamido)benzenate) (Scheme 1) was explored in combination with various [Mn^{III}(SB)]$^+$ Schiff base complexes (SB = saltmen, 5-Me-saltmen, salpen and 3-MeO-salen, with saltmen^{2-} = N,N'-(1,1,2,2-tetramethylethylene)bis(salicylideneiminato) dianion, salpen^{2-} = N,N'-propylenebis(salicylideneiminato) dianion, salen^{2-} = N,N'-ethylenebis(salicylideneiminato) dianion; Scheme 2). In this work, the peripheral substituents of the [Mn(SB)]$^+$ complexes have been modified to investigate their effects on the molecular arrangement of the coordination assembly, on the crystal packing but also on the magnetic coupling between Fe(III) and Mn(III) centers and supramolecular magnetic interactions.

Table 1. Selected Crystal Data and Structural Refinement Parameters of 1–4

	1	2	3	4
formula	$C_{40}H_{39}FeMnN_8O_5$	$C_{34}H_{34}FeMnN_8O_9$	$C_{35}H_{24}FeMnN_8O_4$	$C_{35}H_{30}FeMnN_8O_4$
M/g mol^{-1}	822.58	809.48	695.38	737.46
T/K	150(2)	150(2)	150(2)	150(2)
crystal system	orthorhombic	triclinic	monoclinic	orthorhombic
space group	$Pca2_1$	$P\bar{1}$	$P2_1/c$	$P2_12_12_1$
Z	4	2	4	4
a/Å	23.749(5)	11.548(5)	10.348(5)	10.467(5)
b/Å	8.572(5)	12.431(5)	23.946(5)	12.780(5)
c/Å	18.824(5)	13.160(5)	13.121(4)	24.077(5)
α/deg	90	91.241(5)	90	90
β/deg	90	102.517(5)	116.64(3)	90
γ/deg	90	105.191(5)	90	90
V/Å^3	3832(3)	1773.6(1)	2906.1(18)	3221(2)
d_{calc}/g cm^{-3}	1.426	1.516	1.589	1.521
$F(000)$	1704	834	1420	1516
crystal size	0.30 × 0.24 × 0.21	0.18 × 0.13 × 0.08	0.30 × 0.28 × 0.16	0.25 × 0.21 × 0.18
collected reflections	30669	13259	16618	7303
observed reflections	8767	7999	8512	7303
independent reflections	7302	6172	6777	4167
R_{int}	0.0517	0.0315	0.0217	0.176
data/restraints/parameters	8767/1/503	7999/2/495	8512/0/415	7303/0/446
$R_1{}^a$/$wR_2{}^b$ $(I > 2\,\sigma(I))$	0.0345/0.0789	0.0377/0.0924	0.0374/0.1302	0.0670/0.1450
$R_1{}^a$/$wR_2{}^b$ (all data)	0.0523/0.0995	0.0573/0.1010	0.0675/0.2013	0.1661/0.2269
GOF^c on F^2	1.122	1.050	0.848	1.014
largest diff. peak, hole in e Å^{-3}	0.396, −0.449	1.057, −0.445	1.412, −2.073	1.336, −1.026

$^a R1 = \sum ||F_o| - |F_c||/\sum |F_o|$. $^b wR2 = [\sum w(F_o{}^2 - F_c{}^2)^2/\sum w(F_o{}^2)^2]^{1/2}$; $w = 1/\sigma^2(|F_o|)$. ^{c}Goodness of fit: GOF $= [\sum w(F_o{}^2 - F_c{}^2)^2/(n - p)]^{1/2}$, where n is the number of reflections and p is the number of parameters.

Herein, we report the syntheses, crystal structures, and magnetic properties of seven new cyanido-bridged hetero-bimetallic complexes: two discrete dinuclear compounds [Fe(pcq)(CN)$_3$Mn(saltmen)(CH$_3$OH)]·CH$_3$OH (**1**), [Fe(bpca)(CN)$_3$Mn(3-MeO-salen)(OH$_2$)]·CH$_3$OH·H$_2$O (**2**), and five 1D assemblies [Fe(bpca)(CN)$_3$Mn(salpen)] (**3**), [Fe(bpca)(CN)$_3$Mn(saltmen)] (**4**), [Fe(bpca)(CN)$_3$Mn(5-Me-saltmen)]·2CHCl$_3$ (**5**), [Fe(pcq)(CN)$_3$Mn(5-Me-saltmen)]·2CH$_3$OH·0.75H$_2$O (**6**) and [Fe(bpb)(CN)$_2$Mn(saltmen)]·2CH$_3$OH (**7**). All these compounds were characterized by IR spectroscopy, elemental analysis, and single crystal X-ray structural analysis. Static and dynamic magnetic measurements were also performed to determine the exchange interaction between Fe(III) and Mn(III) ions through a single cyanido bridge and to probe an eventual slow relaxation of the magnetization in these systems.

■ EXPERIMENTAL SECTION

Materials. All chemicals were reagent grade and used as received. 1,3,5-Tris(2-pyridyl)-triazine was purchased from the Aldrich Chemical Co. Hbpca, Hpcq, H$_2$bpb, and [Fe(bpca)$_2$]·H$_2$O were prepared according to literature methods.[19] The precursors [Mn$_2$(saltmen)$_2$]-(ReO$_4$)$_2$, [Mn(salpen)(H$_2$O)](ClO$_4$)·H$_2$O, [Mn$_2$(saltmen)$_2$(H$_2$O)$_2$]-(ClO$_4$)$_2$, [Mn$_2$(5-Me-saltmen)$_2$(H$_2$O)$_2$](ClO$_4$)$_2$, [Mn(3-MeO-salen)-(H$_2$O)](ClO$_4$),[20] (Bu$_4$N)[Fe(bpca)(CN)$_3$],[21] (Ph$_4$P)[Fe(pcq)-(CN)$_3$],[18b] and K[Fe(bpb)(CN)$_2$][22] were prepared according to literature procedures.

Caution! Cyanides are very toxic and should be handled in small quantities and with great caution. Perchlorate salts are potentially explosive. Although no problems were experienced during our experiments, they should be handled in small quantities and with extreme care.

Physical Methods. Elemental analyses for C, H, and N were performed following the classical Pregl-Dumas technique on a ThermoFischer Flash EA1112. FTIR spectra were recorded in the

4000−400 cm^{-1} range on a Nicolet 750 Magna-IR spectrometer using KBr pellets. All the samples were checked by X-ray diffraction prior to any magnetic measurements. Magnetic susceptibility measurements were performed using a Quantum Design MPMS-XL SQUID magnetometer. The measurements were performed on freshly filtered polycrystalline samples introduced in a polyethylene bag (3 × 0.5 × 0.02 cm) except for **5** and **6**, which were covered (and thus restrained) by a minimum of their frozen mother liquor within a sealed straw to prevent desolvation/degradation of the solid during the measurements. No evaporation of the mother liquor was observed during the measurements. The mass of the sample was determined after the measurements and subsequent mother liquor evaporation (CHCl$_3$/CH$_3$OH and CH$_2$Cl$_2$/CH$_3$OH mixtures, respectively). Direct current (dc) measurements were conducted from 300 to 1.8 K and between −70 kOe and 70 kOe applied dc fields. A M vs H measurement was performed at 100 K to confirm the absence of ferromagnetic impurities. The field dependences of the magnetization were measured between 1.8−8 K with dc magnetic field between 0 and 7 T. The alternating current (ac) susceptibility experiments were performed at various frequencies ranging from 1 to 1500 Hz with an ac field amplitude of 3 Oe in zero dc field. Experimental data were corrected for the sample holder and for the diamagnetic contribution of the sample.

Crystallography. Single crystal X-ray crystallographic data were collected on a Nonius Kappa CCD diffractometer with graphite-monochromated Mo−Kα radiation (λ = 0.71073 Å) at 150(2) K for all the compounds. Suitable single crystals were mounted on a glass fiber using silicone grease. DENZO-SMN was used for data integration, and all the data were corrected for Lorentz polarization effects using SCALEPACK.[23] The structures were solved by direct methods and refined by a full-matrix least-squares method on F^2 using the SHELX-TL crystallographic software package.[24] All the atoms were refined anisotropically (except for hydrogen atoms). The H atoms on C atoms were included in calculated positions, whereas H atoms on water molecules were found from the residual peaks and refined with isotropic thermal parameters derived from the parent

Table 2. Selected Crystal Data and Structural Refinement Parameters of 5−7

	5	6	7
formula	$C_{39}H_{36}Cl_6FeMnN_8O_4$	$C_{84}H_{88}Fe_2Mn_2N_{16}O_{11.5}$	$C_{82}H_{76}Fe_2Mn_2N_{16}O_{10}$
M/g mol^{-1}	1004.25	1726.58	1667.17
T/K	150(2)	150(2)	150(2)
crystal system	monoclinic	monoclinic	triclinic
space group	$P2_1/c$	$P2_1/c$	$P\bar{1}$
Z	4	2	4
a/Å	10.795(5)	10.773(3)	17.205(3)
b/Å	13.480(5)	13.759(4)	17.308(4)
c/Å	29.908(5)	27.5931(9)	25.966(5)
α/deg	90	90	91.54(3)
β/deg	96.240(5)	101.672(2)	91.50(3)
γ/deg	90	90	105.14(3)
V/Å^3	4326(3)	4005.4(2)	7457(3)
d_{calc}/g cm^{-3}	1.542	1.427	1.485
$F(000)$	2044	1796	3448
crystal size	0.19 × 0.13 × 0.09	0.21 × 0.17 × 0.09	0.21 × 0.18 × 0.14
collected reflections	17770	31752	47311
observed reflections	9888	9071	26918
independent reflections	5970	5683	20744
R_{int}	0.0559	0.1227	0.0439
data/restraints/parameters	9888/0/538	9071/0/538	26918/0/2041
$R_1{}^a$/w$R_2{}^b$ $(I > 2\ \sigma(I))$	0.0537/0.1351	0.0686/0.1660	0.0896/0.2283
$R_1{}^a$/w$R_2{}^b$ (all data)	0.1111/0.1935	0.1378/0.2231	0.1166/0.2506
GOF^c on F^2	1.014	1.133	1.268
largest diff. peak, hole in e Å^{-3}	0.843, −0.852	1.331, −1.175	1.132, −0.919

$^a R_1 = \sum||F_o| - |F_c||/\sum|F_o|$. $^b wR_2 = [\sum w(F_o{}^2 - F_c{}^2)^2/\sum w(F_o{}^2)^2]^{1/2}$; $w = 1/\sigma^2(|F_o|)$. ^{c}Goodness of fit: GOF $= [\sum w(F_o{}^2 - F_c{}^2)^2/(n - p)]^{1/2}$, where n is the number of reflections and p is the number of parameters.

atoms. Complex **1** crystallizes in the chiral $Pca2_1$ space group (Flack parameter = 0.346). This Flack parameter value should be taken with caution since the crystal was twinned and the TWIN command was used. However, the nature of the enantiomer is not important for our physical properties so the absolute chirality of the compound will not be discussed in the structural description. In complex **2**, no hydrogen atom could be localized on atom O4; whereas based on the bending angle Mn1−O4−C40 (124.2°) and on charge considerations, this axial group is a methanol molecule. Hydrogen atoms on water molecules were not added because of a strong crystallographic disorder of this solvent in complex **6**. Crystallographic data are summarized in Tables 1 and 2, and selected bond lengths and angles of **1−7** are listed in Table 3. Crystallographic data (excluding structure factors) for the structures reported in this paper have been deposited at the Cambridge Crystallographic Data Centre as supplementary publication nos. CCDC-856691 for **1**, CCDC-856692 for **2**, CCDC-856693 for **3**, CCDC-856694 for **4**, CCDC-856695 for **5**, CCDC-856696 for **6**, and CCDC-856697 for **7**. Copies of the data can be obtained free of charge on application to CCDC, 12 Union Road, Cambridge CB21EZ, U.K. (fax: (+44) 1223−336−033; email: deposit@ccdc.cam.ac.uk).

Syntheses. All the complexes have been synthesized using a similar procedure. Therefore, only the synthetic procedure for complex **1** will be described in detail as a representative example for all the complexes.

[Fe(pcq)(CN)₃Mn(saltmen)(CH₃OH)]·CH₃OH (1). A mixture of [Mn₂(saltmen)₂](ReO₄)₂ (250 mg, 0.2 mmol) in methanol (20 mL) was mixed with (Ph₄P)[Fe(pcq)(CN)₃] (124 mg, 0.2 mmol) in 10 mL of dichloromethane. After stirring for 2 h, the resulting dark brown solution was filtered and left undisturbed at room temperature. After 4−5 days, thin brown needle shaped crystals suitable for single crystal X-ray diffraction were obtained. Yield: 53 mg (32%) based on Fe. Anal. Calcd. for C₄₀H₄₀FeMnN₈O₅ (823.58 g mol⁻¹): C 58.35; H 4.74; N 13.62. Found: C 58.28; H 4.8; N 13.53%. IR (KBr) /cm⁻¹: 3421 (m), 2136 (s), 2116 (s), 1636 (s), 1602 (s), 1536 (m), 1500 (m), 1464 (m), 1438 (m), 1389 (m), 1345 (m), 1306 (m).

[Fe(bpca)(CN)₃Mn(3-MeO-salen)(H₂O)]·CH₃OH·H₂O (2). The procedure was the same as for **1** except that [Mn₂(saltmen)₂](ReO₄)₂

and (Ph₄P)[Fe(pcq)(CN)₃] were replaced by [Mn(3-MeO-salen)-(H₂O)](ClO₄) (96 mg, 0.2 mmol) and (Bu₄N)[Fe(bpca)(CN)₃] (124 mg, 0.2 mmol), respectively. Yield: 94 mg (58%) based on Mn. Anal. Calcd. for C₃₄H₃₄FeMnN₈O₉ (809.48 g mol⁻¹): C 50.40; H 4.20; N 13.84. Found: C 50.36; H 4.15; N 13.84%. IR (KBr) /cm⁻¹: 3599 (m), 3511 (m), 3406 (m), 2128 (s), 1713 (s), 1622 (s), 1602 (sh), 1553 (m), 1471 (m), 1442 (s), 1390 (w), 1326 (s).

[Fe(bpca)(CN)₃Mn(salpen)] (3). The procedure was the same as for **1** except that [Mn₂(saltmen)₂](ReO₄)₂ was replaced by [Mn-(salpen)(H₂O)](ClO₄)·H₂O (104 mg, 0.2 mmol) and (Ph₄P)[Fe-(pcq)(CN)₃] was replaced by (Bu₄N)[Fe(bpca)(CN)₃] (124 mg, 0.2 mmol). Yield: 50 mg (36%) based on Mn. Anal. Calcd. for C₃₂H₂₄FeMnN₈O₄ (695.38 g mol⁻¹): C 55.22; H 3.45; N 16.11. Found: C 55.08; H 3.41; N 15.89. IR (KBr) /cm⁻¹: 3428 (m), 2135 (s), 2074 (s), 2046 (s), 1719 (s), 1646 (sh), 1611 (s), 1544(m), 1469 (sh), 1445 (m), 1386 (w), 1319 (s).

[Fe(bpca)(CN)₃Mn(saltmen)] (4). The procedure was the same as for **1** except that (Ph₄P)[Fe(pcq)(CN)₃] was replaced by (Bu₄N)-[Fe(bpca)(CN)₃] (124 mg, 0.2 mmol). Yield: 38 mg (26%) based on Fe. Anal. Calcd. for C₃₅H₃₀FeMnN₈O₄ (737.46 g mol⁻¹): C 56.95; H 4.07; N 15.19. Found: C 56.88; H, 4.17; N 15.17. IR (KBr) /cm⁻¹: 3431 (s), 2138 (s), 2110 (s),1723 (m), 1644 (sh), 1602 (s), 1538 (m), 1468 (m), 1442 (m), 1394 (m).

[Fe(bpca)(CN)₃Mn(5-Me-saltmen)]·2CHCl₃ (5). The procedure was the same as for **1** except that [Mn₂(saltmen)₂](ReO₄)₂ was replaced by [Mn(5-Me-saltmen)(H₂O)](ClO₄) (104 mg, 0.2 mmol) and chloroform was used instead of dichloromethane. Yield: 135 mg (67%) based on Mn. Anal. Calcd. for C₃₉H₃₆Cl₆FeMnN₈O₄ (1004.25 g mol⁻¹): C 46.60; H 3.58; N 11.15. Found: C 46.63; H 3.65; N 11.11. IR (KBr) /cm⁻¹: 3423 (m), 2134 (s), 2112 (s), 1715 (s), 1642 (sh), 1618 (m), 1600 (s), 1540 (m), 1465 (m), 1387 (m), 1320 (sh), 1296 (s).

[Fe(pcq)(CN)₃Mn(5-Me-saltmen)]·2CH₃OH·0.75H₂O (6). The procedure was the same as for **1** except that [Mn₂(saltmen)₂](ReO₄)₂ was replaced by [Mn(5-Me-saltmen)(H₂O)](ClO₄) (104 mg, 0.2 mmol). Yield: 96 mg (56%) based on Fe. Anal. Calcd. for

Table 3. Selected Bond Lengths (Å) and Bond Angles (deg) in 1−7

| 1				2			
Mnl−N6	2.258(3)	Fel−Nl	1.960(3)	Mnl−N6	2.298(2)	Fel−C13	1.938(2)
Mnl−N7	1.997(3)	Fel−N2	1.871(3)	Mnl−N7	1.980(2)	Fel−C14	1.962(3)
Mnl−N8	1.998(2)	Fel−N3	1.966(3)	Mnl−N8	1.9816(18)	Fel−C15	1.955(2)
Mnl−O1	1.892(2)	Fel−C18	1.951(3)	Mnl−O3	1.8867(15)	Fel−Nl	1.959(2)
Mnl−O2	1.886(2)	Fel−C16	1.957(3)	Mnl−O4	1.8773(17)	Fel−N2	1.901(2)
Mnl−O4	2.318(2)	Fel−C17	1.954(3)	Mnl−O7	2.2348(18)	Fel−N3	1.9637(19)
Mn−Fe	5.20			Mn−Fe	5.14		
Fel−C16−N4	174.7(3)			Fel−C14−N4	179.2(2)		
Fel−C18−N6	176.2(2)			Fel−C15−N6	176.8(2)		
Mnl−N6−C18	153.2(2)			Mnl−N6−C15	146.09(18)		
3				**4**			
Mnl−N4	2.360(2)	Fel−Nl	1.9792(19)	Mnl−Nl	2.003(7)	Fel−C21	1.933(7)
Mnl−N6	2.324(2)	Fel−N2	1.891(2)	Mnl−N2	2.000(7)	Fel−C34	1.958(9)
Mnl−N7	2.0072(19)	Fel−N3	1.9612(19)	Mnl−N3	2.302(7)	Fel−C35	1.937(8)
Mnl−N8	2.0092(19)	Fel−C13	1.967(2)	Mnl−N4	2.337(6)	Fel−N6	1.954(7)
Mnl−O3	1.874(16)	Fel−C14	1.948(2)	Mnl−O1	1.896(5)	Fel−N7	1.897(7)
Mnl−O4	1.893(17)	Fel−C15	1.961(2)	Mnl−O2	1.888(5)	Fel−N8	1.974(7)
Mn−Fe	5.15			Mn−Fe	5.28		
Mnl−N4−C13	144.24(18)			Mnl−N4−C21	152.8(6)		
Mnl−N6−C15	151.70(18)			Mnl−N3−C35	153.8(7)		
Fel−C13−N4	173.2(2)			Fel−C21−N4	177.3(7)		
Fel−C15−N6	171.62(19)			Fel−C35−N3	176.1(9)		
5				**6**			
Mnl−N5	2.371(4)	Fel−C13	1.952(4)	Mnl−N5	2.366(4)	Fel−Nl	1.966(4)
Mnl−N6	1.995(3)	Fel−C14	1.972(5)	Mnl−N6	1.998(4)	Fel−N2	1.897(4)
Mnl−N7	2.002(3)	Fel−C15	1.952(5)	Mnl−N7	1.998(4)	Fel−N3	1.964(4)
Mnl−N8	2.314(4)	Fel−Nl	1.959(3)	Mnl−N8	2.305(4)	Fel−C16	1.958(6)
Mnl−O3	1.887(3)	Fel−N2	1.897(3)	Mnl−O1	1.890(4)	Fel−C17	1.969(5)
Mnl−O4	1.887(3)	Fel−N3	1.966(3)	Mnl−O2	1.891(3)	Fel−C18	1.968(5)
Mn−Fe	5.39			Mn−Fe	5.38		
Mnl−N5−C15	162.7(3)			Mnl−N5−C18	160.9(4)		
Mnl−N8−C14	169.7(3)			Mnl−N8−C17	169.4(4)		
Fel−C14−N8	173.0(3)			Fel−C17−N8	174.2(4)		
Fel−C15−N5	176.0(4)			Fel−C18−N5	176.7(4)		
7							
Mn−N$_{ax}$	2.243(6)−2.326(6)	Fe−C	1.951(8)−1.976(7)				
Mn−N$_{eq}$	1.982(5)−2.002(5)	Fe−N	1.884(6)−2.002(6)				
Mn−O	1.880(5)−1.898(5)						
Mn−Fe	5.22						
Mn−N−C	148.9(6)−165.9(7)						
Fe−C−N	166.0(6) −175.1(6)						

$C_{84}H_{91}Fe_2Mn_2N_{16}O_{11.5}$ (1729.58 g mol^{-1}): C 58.28; H 5.26; N 12.95. Found: C 57.86; H 4.70; N 12.97. IR (KBr) /cm^{-1}: 3434 (m), 2129 (s), 1642 (m), 1619 (m), 1598 (s), 1537 (m), 1503 (sh), 1465 (m), 1386 (s), 1344(m), 1305 (m).

[Fe(bpb)(CN)$_2$Mn(saltmen)]·2CH$_3$OH (7). The procedure was the same as for **1** except that (Ph$_4$P)[Fe(pcq)(CN)$_3$] was replaced by K[Fe(bpb)(CN)$_2$] (92 mg, 0.2 mmol). Yield: 68 mg (41%) based on Fe. Anal. Calcd. for $C_{82}H_{76}Fe_2Mn_2N_{16}O_{10}$ (1667.17 g mol^{-1}): C 59.02; H 4.59; N 13.44. Found: C 58.86; H 4.55; N 13.39. IR (KBr) /cm^{-1}: 3434 (m), 2125 (s), 2022 (w), 1604 (s), 1540 (sh), 1468 (sh), 1444 (m), 1394 (m), 1311 (m).

■ RESULTS AND DISCUSSION

Syntheses. Stoichiometric reactions of [Fe^{III}L(CN)$_3$]$^-$ (L = bpca, pcq) or [Fe^{III}(bpb)(CN)$_2$]$^-$ in dichloromethane for **1−4** and **6−7** or chloroform for **5** with a methanolic solution of Mn(III) Schiff base complex led to the formation of heterometallic compounds **1−6** and **7**, respectively. The use of different [Mn(SB)]$^+$ building blocks (SB being saltmen for

1, 4 and **7**, 3-MeO-salen for **2**, salpen for **3** and 5-Me-saltmen for **5** and **6**; see Scheme 2) produced molecular or 1D cyanido-bridged heterobimetallic systems when one or two cyanido groups are in the axial positions of the Mn(III) site, respectively. Single crystals were obtained by slow evaporation of the resulting solutions. It is worth noting that depending on the Schiff base ligand, the Mn(III) precursors crystallize as a mononuclear [Mn(SB)]$^+$ or dimerized [Mn$_2$(SB)$_2$]$^{2+}$ complex.[2a,13,20c,25] Nevertheless in solution, both mono and dinuclear forms are always present and in equilibrium.[20a,26] In this work, when the [Mn(SB)]$^+$/[Mn$_2$(SB)$_2$]$^{2+}$ mixture is reacted with the cyanido-based Fe(III) precursors, only the mononuclear species are obtained in the final compounds in a 1:1 Mn/Fe ratio. It should also be pointed out that **2** has been previously synthesized by Lescouëzec et al. as mentioned in their review[9b] although this compound and its crystallographic structure was not published until now to the best of our knowledge.
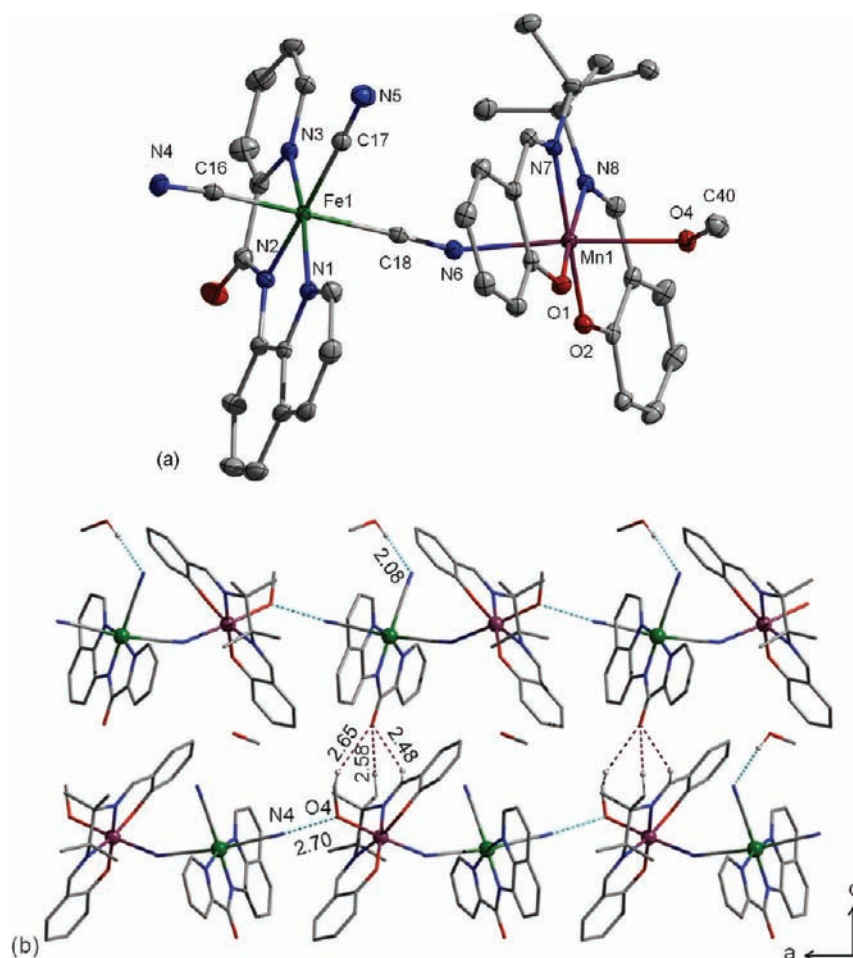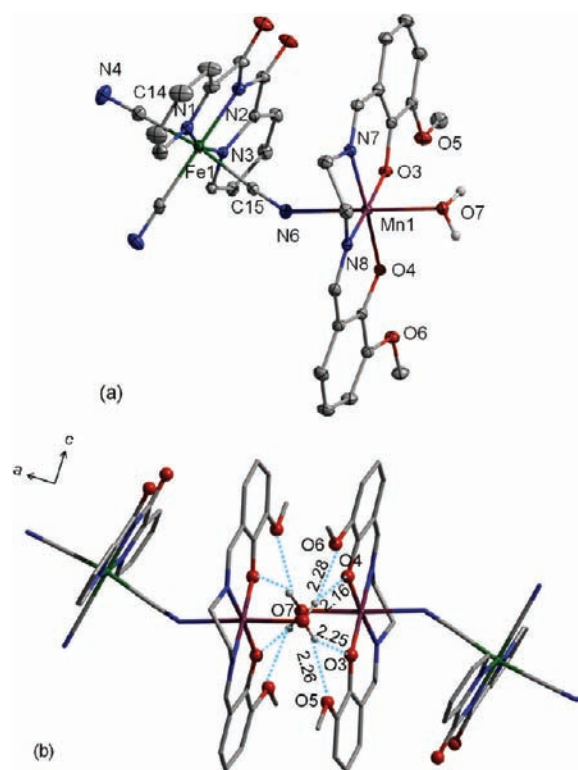
Figure 1. (a) View of the molecular compound **1** with selected atom-labeling schemes and thermal ellipsoids at 30% probability; (b) View emphasizing the 1D arrangement of **1** along the *a* axis through H bonds (cyan dashed lines). Short range interactions and hydrogen bonds are respectively visualized by purple dotted and cyan dashed lines. All H atoms are omitted for clarity.

The infrared spectra of all these systems present the typical bands of the Fe(III) and Mn(III) precursors. Strong characteristic $\bar{\nu}$(CN) bands are observed in the range 2140−2125 cm^{-1} (2136, 2128, 2135, 2138, 2134, 2129, and 2125 cm^{-1} for **1**, **2**, **3**, **4**, **5**, **6**, and **7**, respectively) and are shifted to higher energies compared to the ferric building block (2122 cm^{-1} for [Fe^{III}(bpca)(CN)$_3$]$^-$,[21] 2117 and 2059 cm^{-1} for [Fe^{III}(pcq)-(CN)$_3$]$^-$,[18b] and 2114 cm^{-1} for [Fe^{III}(bpb)(CN)$_2$]$^-$).[22] The $\bar{\nu}$(CN) shifts are an unambiguous indication that cyanido groups bridge both transition metal ions in **1−7**.[27] Furthermore, the strong peak around 1605 cm^{-1} present in all the complexes is assigned to the terminal C≡N stretching vibration from the Schiff base ligands. Peaks centered around 3060, 2950, 1090, or 920 cm^{-1} were not detected in the IR spectra indicating respectively the absence of PPh$_4$$^+$, Bu$_4N^+$, ClO$_4$$^-$ or ReO$_4$$^-$ counterions in the structures. The analysis of the IR spectra suggests the formation of stable neutral systems by charge compensation between the [Fe(L)(CN)$_x$]$^-$ anion and the [Mn(SB)(H$_2$O)]$^+$ cation in an equimolar ratio, as confirmed by the crystal structures described in the next section.

Structural Descriptions. The structures of **1−7** have been determined by single crystal X-ray diffraction technique. Crystallographic data for all the complexes are listed in Tables 1 and 2 while selected bond lengths and angles are summarized in Table 3.

Complexes 1 and 2. Single crystal X-ray diffraction studies revealed that **1** and **2** crystallize in the orthorhombic *Pca*2$_1$ and the triclinic *P*$\bar{1}$ space groups and are discrete dinuclear complexes resulting from the assembly of a [Fe(L)(CN)$_3$]$^-$ anionic precursor (L = pcq for **1** and bpca for **2**) and a [Mn(SB)(S)]$^+$ (SB = saltmen and S = MeOH for **1**; SB = 3-MeO-salen and S = H$_2$O for **2**) cationic moiety linked by a single CN bridge. Their crystallographic structures are depicted in Figures 1 and 2, respectively. Two cyanido groups from the [Fe(L)(CN)$_3$]$^-$ unit are uncoordinated and a solvent molecule is coordinated to the Mn(III) center in *trans*-position to the bridging CN group, resulting in discrete species as shown in Figures 1a and 2a. The Mn centers in **1** and **2** adopt an elongated distorted octahedral environment, emphasizing the characteristic Jahn−Teller effect observed for Mn(III) metal ions. The Mn(III) equatorial plane is defined by two N atoms (Mn1−N$_{eq}$ = 1.997(3)−1.998(2) Å for **1** and 1.980(2)−1.9816(18) Å for **2**) and two phenolato O atoms of the Schiff base ligands (Mn1−O = 1.886(2) and 1.892(2) Å for **1** and 1.8773(17) and 1.8867(15) Å for **2**) while the axial positions are occupied by one bridging cyanido ligand (Mn1−N6 = 2.258(3) Å for **1** and 2.298(2) Å for **2**) and one solvent molecule (Mn1−OH(CH$_3$) = 2.318(2) Å for **1** and Mn1−O$_w$ = 2.2348(18) Å for **2**). The Mn−N−C angles of the cyanido bridge are 153.2(2)° for **1** and 146.09(18)° for **2**. The methanol molecule in axial position in **1** is quite bent with a

Figure 2. (a) View of the molecular compound **2** with selected atom-labeling scheme and thermal ellipsoids at 30% probability; (b) View illustrating the pairing of the dinuclear complexes in **2** induced by H bonds (blue dashed lines) between coordinated water molecules and oxygen atoms of the adjacent Schiff base ligands. All H atoms are omitted for clarity.
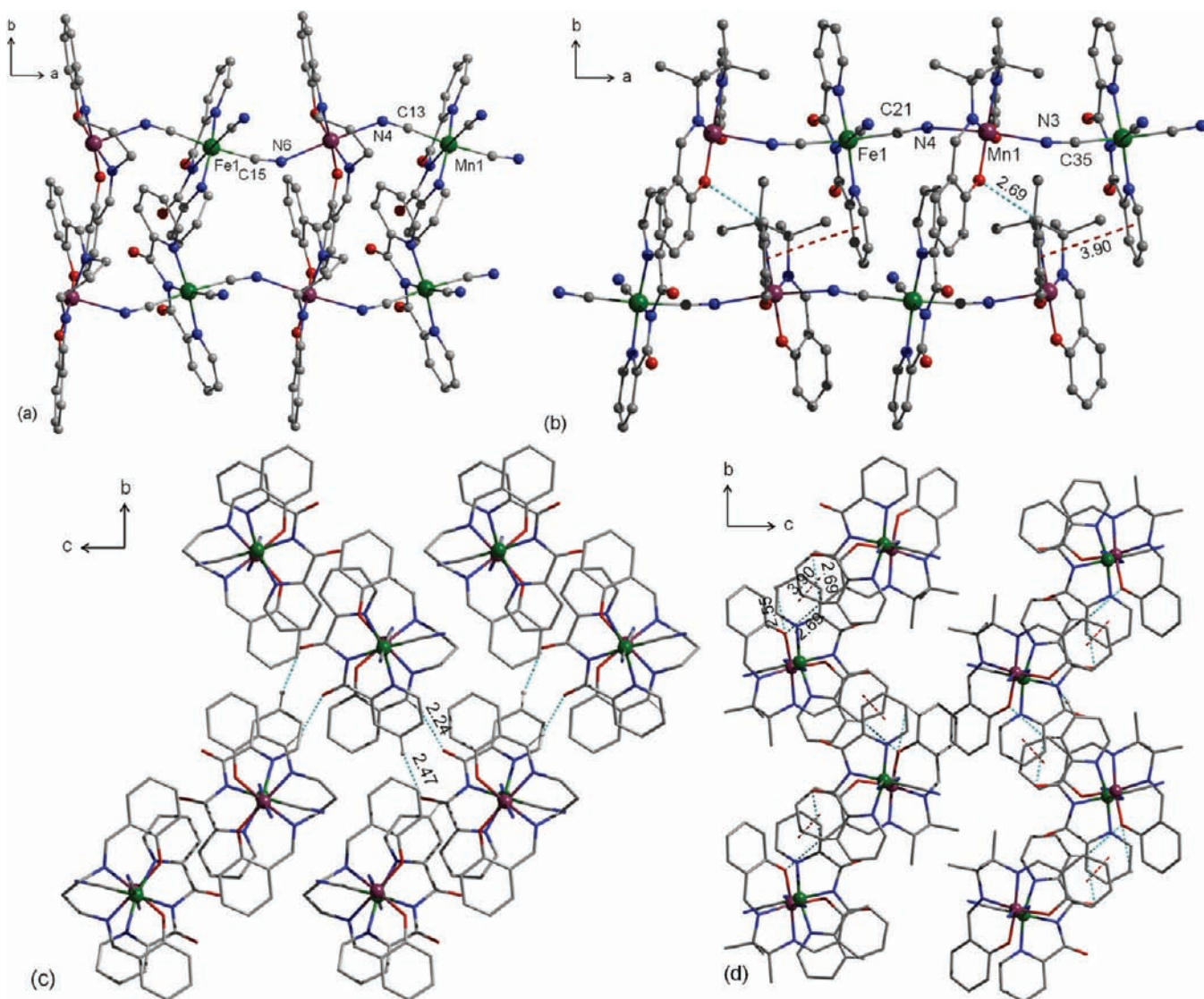
Mn1−O4−C40 angle of 124.2(2)°. The Fe(III) coordination sphere can be described as a distorted octahedron with three N atoms from the L capping ligand and three C atoms from CN groups. The equatorial Fe−N and Fe−C($\equiv$N) bond lengths are similar in both complexes (Fe1−N = 1.871(3)−1.966(3) Å; Fe1−C17 = 1.954(3) Å for **1** and Fe1−N = 1.901(2)−1.964(2) Å; Fe1−C13 = 1.938(2) Å for **2**). The axial Fe−C($\equiv$N) distances are Fe1−C16 = 1.957(3) Å; Fe1−C18 = 1.951(3) Å for **1** and Fe1−C14 = 1.962(3) Å; Fe1−C15 = 1.955(2) Å for **2**. These distances are in agreement with other low-spin Fe(III) complexes described in the literature.[14a,18d,e,21] The Fe−C−N angles only slightly deviate from 180° (176.2° for **1** and 176.8° for **2**) while the intramolecular distances between Fe and Mn centers are 5.20 Å for **1** and 5.14 Å for **2**.

An inspection of the packing in **1** revealed the association of the neutral heterobimetallic units through hydrogen bond interactions between the protonated oxygen (O4) of the coordinated methanol molecule and the nitrogen atom (N4) of a terminal cyanido ligand (O4···N4 = 2.70 Å). These H-bond interactions afford a supramolecular chain along the *a* axis (Figure 1b) while non coordinated methanol molecules interact with the equatorial uncoordinated nitrogen atom of the CN group (O5−H5···N5 = 2.08 Å). In the crystal packing, additional short intermolecular interactions are present between supramolecular chains (Figure 1b) promoting a close packing in the *bc* plane (Supporting Information, Figure S1). The shortest interdinuclear Mn···Fe distance in **1** is 7.26 Å and 8.57 Å for Mn···Mn and Fe···Fe distances. In **2**, terminal water molecules (O7) present in the axial positions of the Mn(III) ion (instead of the methanol group in **1**) are involved

in hydrogen bonds with the methoxido-(O5 and O6) and phenolato-(O3 and O4) oxygen atoms of the Mn (III) Schiff base ligand from an adjacent dinuclear unit generated by the inversion center (Figure 2b, O···H = 2.16−2.28 Å). It is worth noting that, based on previous examples of Mn(III)−NC−Fe(III) compounds, 3-MeO-salen was found to promote similar supramolecular dimers of dinuclear species[14a,18d,28] and compound **2** further confirms this tendency. **2** is then best described as a tetranuclear entity with an intermetallic Mn(1)···Mn(1*) (* = −x, 1−y, 1−z) separation equal to 4.76 Å and this short contact between Mn sites will have important consequences on its magnetic properties (see below). In the extended network, heterobimetallic units are further associated through hydrogen bonds between crystallized water molecules and oxygen atoms from the carbonyl group of the bpca ligand (H···O = 2.19−2.32 Å), resulting in chains of tetranuclear units running along the *a* axis (Supporting Information, Figure S2).

Complexes 3−6. Compounds **3−6** were prepared in the same synthetic conditions as the previous discrete compounds (**1** and **2**) and all crystallize in the monoclinic $P2_1/c$ space group except compound **4**, which crystallizes in the orthorhombic $P2_12_12_1$ space group. The cyanido-based Fe(III) building blocks behave as linkers between [Mn^{III}(SB)]$^+$ units (as suggested by IR spectroscopy) leading to the formation of neutral 1D arrangements of alternating [Fe^{III}L(CN)$_3$]$^-$ (L = bpca for **3−5** or pcq for **6**) and [Mn^{III}(SB)]$^+$ units linked through two cyanido groups in *trans*-positions. In Figures 3 and 4, the chain structures are represented along and perpendicular to the *a* direction to visualize their three-dimensional (3D) packing. The asymmetric unit of compounds **3−6** is shown in Supporting Information, Figures S3 and S4. It should be highlighted that all the chains built from [Fe(bpca)(CN)$_3$]$^-$ and [Fe(pcq)(CN)$_3$]$^-$ involve two bridging cyanido groups in *trans*-positions; whereas until now, most of the chains incorporating tricyanido *mer*-Fe(III) precursors and Mn(III) complexes displayed a zigzag arrangement involving two bridging cyanido groups in *cis* positions,[18c−e] with the exception, to the best of our knowledge, of five complexes: [Mn((R,R)-salcy)Fe(bpca)(CN)$_3$(H$_2$O)]$_n$, [Mn((S,S)salcy)Fe-(bpca)(CN)$_3$(H$_2$O)]$_n$, [Fe(iqc)(CN)$_3$Mn-(salen)]·MeCN·H$_2$O, [Fe(iqc)(CN)$_3$Mn(5-F-salen)]·MeOH·1.5H$_2$O, and [Fe(iqc)(CN)$_3$Mn(5-Cl-salen)]·MeOH·1.5H$_2$O (with (R,R)-salcy or (S,S)-salcy: (R,R)-or (S,S)-N,N-(1,2-cyclohexanediylethylene)bis-(salicylideneiminato) dianion ; Hiqc: N(quinolin-8-yl)-isoquinoline-1-carboxamide).[29]

The Fe(III) ion is located in a slightly distorted octahedral environment defined by the tridentate N-donor ligand bis(2-pyridylcarbonyl)amidate and three cyanido ligands (one CN group is uncoordinated). The Fe(1)−C($\equiv$N) bond lengths are very similar in these compounds and are in the range 1.948(2)−1.967(2) Å for **3**, 1.933(7)−1.958(9) Å for **4** and 1.952(4)−1.972(5) Å for **5**, 1.958(6)−1.969(5) Å for **6** (see Table 3). They are in good agreement with those observed in other cyanido-based low-spin iron(III) complexes reported in the literature.[14a,18d,e,21] The Fe−N bond distances are also similar for all these complexes (Fe(1)−N = 1.891(2)−1.9792(19) Å for **3**, 1.897(7)−1.974(7) Å for **4**, 1.897(3)−1.966(3) Å for **5**, 1.897(4)−1.966(4) Å for **6**). Finally, the Fe−C($\equiv$N) bridging angles are close to 180° (171.6(2)° and 173.2(2)° for **3**, 176.1(9)° and 177.3(7)° for **4**, 173.0(3)° and 176.0(4)° for **5**, 174.2(4)° and 176.7(4)° for **6**). The Mn(III)
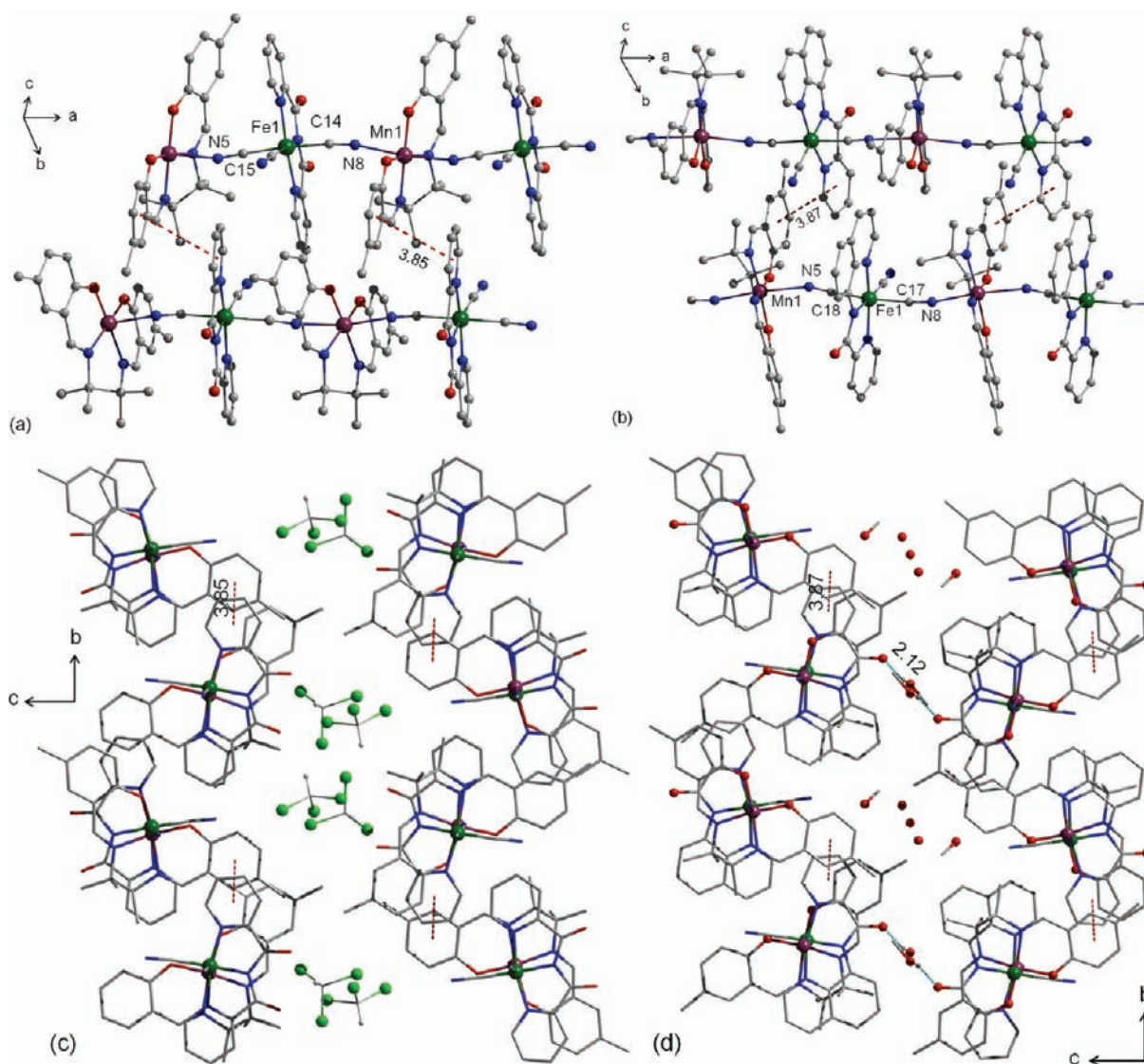
Figure 3. Ball and stick views illustrating pairs of chains in the *ab* plane in compounds **3** (a) and **4** (b). Crystal packing perpendicular to the *a* axis for **3** (c) and **4** (d). Mn, Fe, N, O, and C atoms are represented in purple, green, blue, red, and gray, respectively. All H atoms are omitted for clarity except to visualize H-bond interactions. Weak $\pi-\pi$ and H-bond interactions are indicated with red dotted and blue dashed lines, respectively.

ion is well described as a Jahn–Teller elongated octahedron with the four equatorial N_2O_2 donor atoms originating from the Schiff base ligand (Mn(1)–N_{eq} = 2.0072(19)–2.0092(19) Å for **3**, 2.000(7)–2.003(7) Å for **4**, 1.995(3)–2.002(3) Å for **5**, 1.998(4) Å for **6**; Mn(1)–O_{eq} = 1.874(16)–1.893(17) Å for **3**, 1.888(6)–1.896(5) Å for **4**, 1.887(3) Å for **5**, 1.890(4)–1.891(3) Å for **6**) and two apical N atoms coming from the cyanido groups of two neighboring $[Fe(L)(CN)_3]^-$ moieties (Mn(1)–N_{ax} = 2.324(2) and 2.360(2) Å for **3**, 2.302(7) and 2.337(6) Å for **4**, 2.314(4) and 2.371(4) Å for **5**, 2.305(4) and 2.366(4) Å for **6**). The Mn(1)–N≡C angle values in the bridging pathways are equal to 144.24(18)° and 151.70(18)° for **3**, 152.8(6)° and 153.8(7)° for **4**, 162.7(3)° and 169.7(3)° for **5**, 160.9(4)° and 169.4(4)° for **6**. These angles deviate significantly from the linearity compared to the almost linear Fe–C(≡N) angles as usually observed in similar systems.[14b,18e,21,29] From these angle values, the chains **3** and **4** appear significantly corrugated whereas **5** and **6** display a more linear 1D arrangement. These structural differences may be related to the presence or absence of substitution on the

salen type ligand that might tune both packing (vide infra) and geometry of the chains. Indeed, **3** and **4** incorporate unsubstituted Schiff Base ligands while **5** and **6** contain 5-Me-saltmen ligands. The presence of methyl on the 5-position of the phenyl groups of the saltmen ligand in **5** and **6** seems to induce a quasi-linear arrangement independently of the capping ligand on the tricyanido *mer*-Fe(III) unit (bpca for **5** and pcq for **6**). Finally, it is interesting to note that the shortest intrachain distance between Fe and Mn centers in **3**–**6** are very similar between 5.15 and 5.39 Å (Table 3).

It is important to compare the packing arrangements of the chains to detect supramolecular interactions that could induce interchain magnetic couplings, which are an important parameter in analyzing the magnetic properties of the compounds. It is worth noting that the crystal structures of **3** and **4** do not contain interstitial solvent molecules while two chloroform molecules are present in **5** and two methanol and a water molecule with an occupancy of 0.75 are found in **6**. In these four compounds **3**–**6**, chains systematically form pairs in similar 3D arrangements (Figures 3c, 3d, 4c and 4d). For
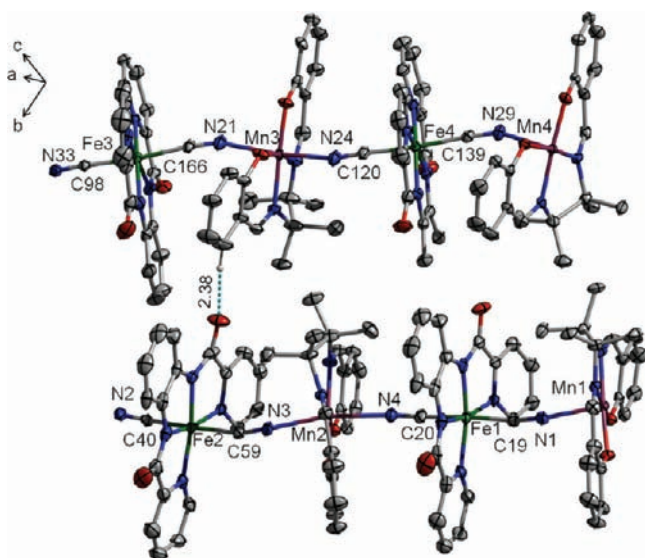
Figure 4. Ball and stick views illustrating the formation of chain pairs in compounds **5** (a) and **6** (b). Crystal packing perpendicular to the *a* axis for **5** (c) and **6** (d). Mn, Fe, N, O, and C atoms are represented in purple, green, blue, red, and gray, respectively. All H atoms are omitted for clarity except to visualize H-bond interactions. Weak $\pi-\pi$ interactions and hydrogen bonds are indicated with red dotted and cyan dashed lines, respectively.

instance, a deep structural inspection of **3** revealed the presence of short contact interactions through van der Waals forces between terminal oxygen atoms of the bpca ligand and hydrogens from phenyl (H···O = 2.47 Å) and imine (H···O = 2.24 Å) groups on the salpen ligand. Adjacent Mn(III) centers are thus located side to side in a ladder type arrangement (Figure 3a, Mn···Mn = 7.39 Å). No $\pi-\pi$ interactions are detected inside and between the ladders but short H···O and H···N contacts between chains generate a well-packed 3D network (Figure 3c). Weak interchain interactions are also detected between adjacent chains in **4** giving rise to a similar ladder-like arrangement (Figures 3b and 3d) interacting via weak $\pi-\pi$ interactions (centroid to centroid distance = 3.90 Å) to form layers of ladders in the *bc* plane. Further H···O contacts are present in these layers with H···O distances superior to 2.5 Å. $\pi-\pi$ interactions between saltmen and bpca aromatic rings result in a long Mn···Mn separation of 8.82 Å since adjacent Mn(III) centers are shifted between two neighboring chains (Figures 3a and 3b).

Finally, the quasi-linear chains in compounds **5** and **6** are also arranged by pairs through short $\pi-\pi$ contacts (centroid to centroid distance = 3.85 and 3.87 Å, respectively). Pairs of chains are packed in layers perpendicular to the *a* axis similarly to **3** and **4** as emphasized in Figures 4c and 4d via short H-bond interactions (2.37–2.98 Å and 2.48–2.88 Å, respectively). Nevertheless, the crystal packing for **5** and **6** are quite different in comparison to **3** and **4** because of solvent molecules intercalated between these layers of chains in parallel to the *ab* plane. While in **5**, CHCl$_3$ molecules ensure an efficient isolation of the layers (see Figure 4c), hydrogen bond interactions are present in **6** between terminal oxygen of the pcq ligand and hydrogen atoms from cocrystallized methanol molecules (H···O = 2.12 Å, Figure 4d). The shortest interchain Fe···Mn, Mn···Mn, and Fe···Fe distances are respectively 7.67, 7.39 and 7.73 Å for **3**; 8.21, 8.81 and 8.33 Å for **4**; 7.52, 7.73 and 7.77 Å for **5** and 7.68, 7.78 and 7.89 Å for **6**.

Complex 7. A single crystal X-ray diffraction analysis showed that complex **7** crystallizes in the triclinic $P\bar{1}$ space group. It is

important to recall first that complex **7** was synthesized with the *trans*-dicyanido ferric building block, $[Fe(bpb)(CN)_2]^-$, whereas, in the case of **1−6**, tricyanido *mer*-Fe(III) precursors were used. From a crystallographic point of view, **7** is also different compared to **3−6** as two crystallographically independent but parallel chains run along the *a+b* direction as illustrated by Figure 5. The 1D assembly consists of [-NC-Fe(bpb)-CN-
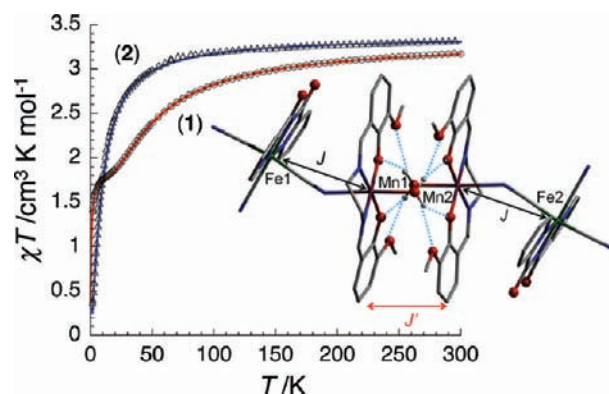

Figure 5. Molecular structure of **7** with selected atom-labeling schemes and thermal ellipsoids at 50% probability. Mn, Fe, N, O, and C atoms are represented in purple, green, blue, red, and gray, respectively. All H atoms are omitted for clarity, and hydrogen bonds are indicated with cyan dashed lines.

Mn(saltmen)] repeating motifs with each cyanido group connected to the Mn(III) Schiff Base complex in axial positions. All the Mn centers are hexacoordinated in an elongated distorted octahedral environment. Their equatorial positions are occupied by two N atoms ($Mn-N_{eq}$ ranging from 1.984(5) to 2.002(5) Å) and two O atoms from the saltmen ligand ($Mn-O$ distances between 1.880(5) and 1.897(5) Å). On the other hand, two terminal nitrogen atoms from the $[Fe(bpb)(CN)_2]^-$ moieties are coordinated to the Mn(III) axial positions ($Mn-N$(cyanido) = 2.242(6) to 2.328(5) Å). In the $[Fe(bpb)(CN)_2]^-$ unit, the Fe(III) sites also have a distorted octahedral environment defined by two cyanido ligands in *trans* position and the tetradentate *N*-donor ligand bpb^{2-} (Scheme 1), in the equatorial plane. The Fe−N(bpb) (1.887(6)−2.003(5) Å) and Fe−C(≡N) (1.951(6)−1.977(6) Å) bond lengths are in good agreement with the previous reported low-spin $\{Fe(bpb)(CN)_2\}$ unit,[15a−e] and other cyanido-based low-spin iron(III) complexes.[30] The Mn−N≡C bond angles range between 148.8(5) and 166.0(6)° while the shortest intrachain distance between Fe and Mn centers is 5.22 Å. In the crystal structure of **7**, hydrogen bonds occur between the terminal carbonyl group of the bpb ligand and methanol solvent molecules (H···O = 1.98−2.55 Å, see Supporting Information, Figure S5a). Short contacts between the crystallographically identical chains (between phenolato O atoms of the saltmen ligand and pyridine H atoms of the bpb ligand or phenyl H atoms of a neighboring saltmen ligand: H···O-(phenolato) = 2.21−2.50 Å) along the *a+b* direction promote the formation of a supramolecular pair of chains (Supporting Information, Figures S5b and S5c). Only one type of additional

short contact interactions (<2.5 Å) was detected between crystallographically independent paired chains involving carbonyl O atoms of the bpb ligand and H atoms of saltmen ligands (H···O = 2.38 Å). The shortest interchain Fe···Mn, Mn···Mn, and Fe···Fe distances for **7** are 7.02, 7.39 and 7.20 Å, respectively.

Magnetic Properties. *Complexes 1 and 2.* The dc magnetic susceptibility data of **1** and **2** were measured on polycrystalline samples. At room temperature, the χT product is 3.2 and 3.3 cm^3 K mol^{-1} for **1** and **2**, respectively, in good agreement with the theoretical value of 3.375 cm^3 K mol^{-1} for one Fe(III) (s_{Fe} = 1/2) and one Mn(III) (S_{Mn} = 2) isolated spin carriers assuming g_{Fe} = g_{Mn} = 2.0. Decreasing the temperature, the χT product at 1000 Oe gradually decreases to reach a minimum value of 1.3 and 0.3 cm^3 K mol^{-1} at 1.8 K respectively (Figure 6 and Supporting Information, Figure S6).

Figure 6. Temperature dependence of the χT product at 1000 Oe for **1** (circles) and **2** (triangles). Solid red and blue lines indicate the best fits obtained with the model described in the text. Inset: Representation of the spin and magnetic interaction topologies for **2**.

This thermal behavior indicates the presence of an antiferromagnetic interaction between s_{Fe} = 1/2 Fe(III) and S_{Mn} = 2 Mn(III) spin carriers that should result in an S_T = 3/2 spin ground state. This ground state is confirmed by the *M* vs *H* data (Supporting Information, Figure S7) and the magnetization at 1.8 K under 7 T that reaches 2.4 and 2.7 μ_B for **1** and **2**, respectively, in good agreement with the expected saturation value of 3 μ_B (for S_T = 3/2). In the low temperature region and for both compounds, χT does not stabilize to 1.875 cm^3 K mol^{-1} expected for an S_T = 3/2 spin ground state, suggesting the presence of intercomplex antiferromagnetic interactions. Indeed, **1** exhibits a quasi-plateau of χT around 13 K at 1.8 cm^3 K mol^{-1} in agreement with the expected value but an additional decrease of the χT product is observed at lower temperatures. For **2**, the decrease of the χT product is much stronger than for **1** indicating stronger intermolecular antiferromagnetic interactions for **2**. As shown in the structural description of these compounds (vide supra), intermolecular interactions arising from hydrogen bonds are present in the crystal packing connecting dinuclear complexes and leading to 3D supramolecular assemblies for **1** and **2** (Figure 1b, Supporting Information, Figures S1 and S2) in addition to a strong dimerization of the complexes in **2** (Figure 2b). This latter feature is certainly responsible for the presence of stronger antiferromagnetic interactions between dinuclear moieties in **2**.

To determine the intra- and interdimer exchange constants (*J* and *zJ*′, respectively) between the Fe(III) and Mn(III)

paramagnetic ions ($S_{Mn} = 2$ and $s_{Fe} = 1/2$) in **1**, an isotropic Heisenberg dimer model was used with the following spin Hamiltonian:

$$H = -2J(S_{Mn} \cdot s_{Fe})$$ (1)

while the intermolecular interactions have been treated in the mean field approximation.[31] Using the deduced susceptibility (χ_{MnFe}, eq 2) from this Heisenberg model, an acceptable simulation of the χT vs T data has been obtained in the 300–1.8 K range with $J/k_B = -16.1(2)$ K, $g = 2.0(1)$, and $zJ'/k_B = -0.24(2)$ K.

$$\chi T_{MnFe} = \frac{Ng^2\mu_B^2}{k_B} \cdot \frac{(10 + 35 \exp(5J/k_BT))}{4(2 + 3 \exp(5J/k_BT))}$$ (2)
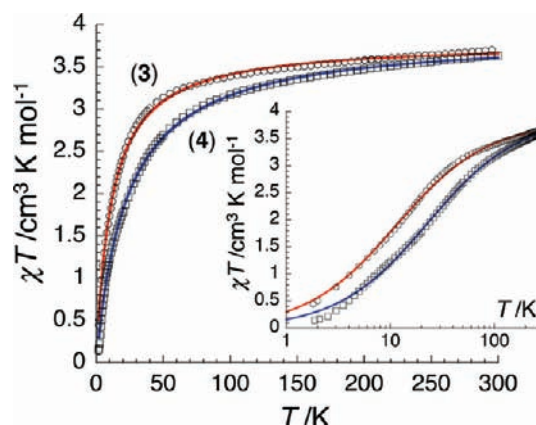
The obtained magnetic parameters are consistent with the values reported in other dinuclear Fe(III)–Mn(III) complexes made of tricyanido mer-Fe(III) building blocks.[18d,e] It is also important to mention that at $T < 20$ K, the magnetic anisotropy of the Mn(III) centers is usually relevant to describe the magnetic properties of such complexes, thus the zJ' value is likely overestimated by this contribution. Moreover, it is worth noting that a magnetic model considering only the Mn(III) anisotropy[32] instead of the intercomplex magnetic interactions does not lead to an acceptable fit of the experimental data. Since these data are already well modeled with intercomplex interactions, an overparametrization of the modeling procedure is observed when both anisotropy and zJ' are considered. Hence, the anisotropy was finally neglected in our model.

In **2**, only the magnetic exchange between Mn(III) and Fe(III) spin carriers through the CN bridge and between Mn(III) centers of the two neighboring dinuclear complexes through short H-bonds involving coordinating water molecules (shown in Figure 2b and Figure 6 inset) have been considered as a first approximation in the magnetic model. Thus, the following spin Hamiltonian, eq 3,

$$H = -2J(S_{Mn1} \cdot s_{Fe1} + S_{Mn2} \cdot s_{Fe2}) - 2J'(S_{Mn1} \cdot S_{Mn2})$$ (3)

(with $S_{Mn1} = S_{Mn2} = 2$, $s_{Fe1} = s_{Fe2} = 1/2$, J being the magnetic interaction between Mn(III) and Fe(III) centers and J' being the magnetic interaction between Mn(III) metal ions) has been used to calculate[32] the magnetic susceptibility of the tetranuclear entity shown Figure 6 inset. Both χT vs T (Figure 6 and Supporting Information, Figure S6) and M vs H (Supporting Information, Figure S7) data have been simultaneously well simulated with the following set of parameters: $J/k_B = -3.5(1)$ K, $J'/k_B = -0.81(3)$ K, and $g = 2.0(1)$. The obtained values of the magnetic exchange are comparable to those reported in similar arrangements.[14a,18d,28b] It is worth noting that the antiferromagnetic nature of the J' interaction induces an overall diamagnetic ground state of the tetranuclear supramolecular assembly.

Complexes 3 and 4. The static magnetic properties of **3** and **4** have been studied and are shown in Figure 7 as the temperature dependence of the χT product. The χT value at room temperature is equal to 3.7 and 3.6 cm^3 K mol^{-1}, respectively, which is in good agreement with the expected χT value of 3.375 cm^3 K mol^{-1} calculated for one low spin $s_{Fe} = 1/2$ Fe(III) center and one $S_{Mn} = 2$ high spin Mn(III) metal ion assuming $g_{Fe} = g_{Mn} = 2.0$. When the temperature is decreased, the χT product decreases down to 0.44 and 0.14 cm^3 K mol^{-1} at 1.8 K for **3** and **4**, respectively. This thermal behavior is

Figure 7. Temperature dependence of the χT product at 1000 Oe for **3** and **4**. Inset: Semi-logarithmic plot of χT vs T in the 300–1.8 K temperature range. The solid lines represent the best fits obtained with the models described in the text.

typical of dominant antiferromagnetic interactions between the Mn(III) and Fe(III) spin carriers as already observed in **1** and **2**. To estimate the magnitude of these exchange interactions within the chain, the experimental data of **3** and **4** have been modeled using an isotropic Heisenberg Hamiltonian (eq 4, with $S_{Mn,i} = S_{Mn,i+1} = 2$ and $s_{Fe,i} = 1/2$) based on the Seiden approach for alternating chains of quantum spins $s = 1/2$ and classical spins $S = 2$.[33]

$$H = -2J \sum_{-\infty}^{+\infty} (S_{Mn,i} \cdot s_{Fe,i} + s_{Fe,i} \cdot S_{Mn,i+1})$$ (4)
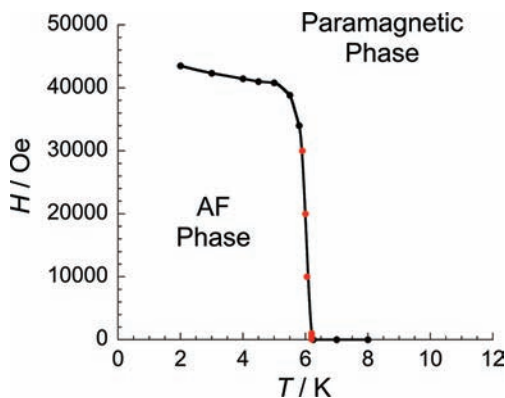
For both compounds, this model was unable to fit the experimental data down to 1.8 K. Nevertheless, the Seiden model could reproduce the data above 50 K clearly suggesting a dominant 1D behavior in this temperature range with J/k_B of the order of −4 and −10 K for **3** and **4**, respectively.

To reproduce the experimental data below 50 K, interchain exchange interactions (J') were introduced in the model in the mean field approximation.[31] This approach led to multiple (J, J') solutions with a general trend to have similar negative values for J and J' with the intrachain interaction being systematically slightly larger than the interchain coupling. Therefore, these compounds are structurally 1D coordination polymers (Figures 3a and 3b) but are better described as 3D networks from a magnetic point of view at least below 50 K. The structural analysis of these compounds also supports the 3D nature of the magnetic interaction networks as shown by the close packed arrangements of chains in **3** and **4** (Figures 3c and 3d). This is actually confirmed by the fit of the experimental data to a Curie–Weiss law that almost perfectly matches down to 1.8 K with Curie constants of 3.8(1) and 3.9(1) cm^3 K mol^{-1} and Weiss temperatures of −11.4(5) and −22.9(5) K, respectively (Figure 7). It is worth noting that these Curie constants lead to average g values of about 2.1, and these Weiss constants further confirm the presence of dominating antiferromagnetic interaction between spin carriers.

M vs H measurements have also been performed below 10 K for both compounds (Supporting Information, Figure S8). At high fields, even under 7 T and at 1.8 or 2 K, the magnetization is not saturated, reaching 2.72 and 2.25 μ_B for **3** and **4** respectively. These high field values are in good agreement with an antiferromagnetic arrangement of the $S_{Mn} = 2$ Mn(III) and

s_{Fe} = 1/2 Fe(III) spins along the chain (a saturated magnetization around 3 μ_B is expected for antiferromagnetic intrachain interactions). Furthermore, the magnetization exhibits very similar field dependence with a typical "*S*" shape curve (i.e., with an inflection point) at 1.8 K that reveals the presence of antiferromagnetic interactions between chains compensated by the applied magnetic field at H_C. This characteristic field has been followed as a function of the temperature using combined *M* vs *H* and χ vs *T* data (Supporting Information, Figures S8, S9 and S10) and taking the maximum of the d*M*/d*H* vs *H* and χ vs *T* plots.

Using this approach, the (*T*, *H*) magnetic phase diagram has been built for **4** (Figure 8), while for **3**, H_C is observed around

Figure 8. *H* vs *T* magnetic phase diagram for **4**. The black and red dots are respectively the experimental points deduced from the *M* vs *H* and χ vs *T* data (Supporting Information, Figure S10). The solid black line is a guide for the eye.

21000 Oe only at 1.8 and 2 K and disappears at higher temperatures providing an insufficient set of data to accurately establish its magnetic phase diagram. These results prove the presence of an antiferromagnetic 3D magnetic order in both compounds with T_N = 2−3 and 6.2 K for **3** and **4**, respectively. The topology of the phase diagram obtained for **4** is typical of a metamagnetic behavior with only an antiferromagnetic−paramagnetic phase transition that is certainly induced by the magnetic anisotropy brought by the Mn(III) metal ions (note that an intermediate spin-flop phase is usually observed for antiferromagnetic materials that possess a weak anisotropy). From the critical field extrapolated at 0 K (H_c^0), which is equal to 21000 and 43000 Oe for **3** and **4**, respectively, it is possible to estimate the average antiferromagnetic interactions between effective S_{eff} = 3/2 spins constituting the antiferromagnetic coupled chain using the following expression:[34]

$$g\mu_B H_C^0 S_{eff} = 2|zJ'|S_{eff}^2 \qquad (5)$$

The value of zJ'/k_B is thus estimated at −1.0 and −2.0 K for **3** and **4**, which confirms the existence of strong interchain interactions responsible for the antiferromagnetic phase transition. In the frame of the mean field approximation, the theoretical Néel temperature (T_N) can be estimated at 2.5 and 5 K for **3** and **4**, respectively, from these average interchain magnetic interactions (zJ'/k_B) and using the following well-known relation:

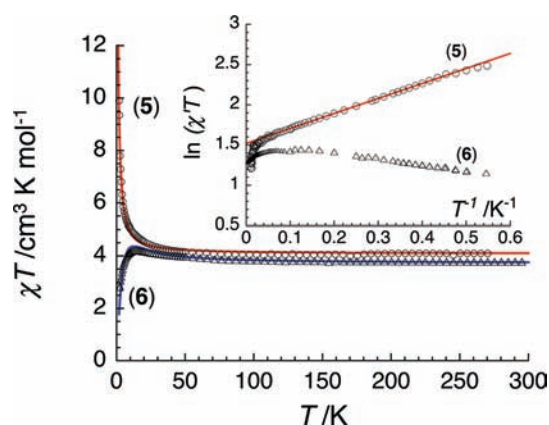$$T_N = 2|zJ'|S_{eff}(S_{eff} + 1)/3k_B \qquad (6)$$

For **4**, the experimental T_N is clearly underestimated by this approach as expected when the intrachain interactions are

stronger than the interchain interactions. The critical temperature is also probably underestimated for **3** but it is clearly in agreement with the experimental data that located the transition between 2 and 3 K.

The magnetic properties of these two compounds are also well understood from a structural point of view particularly the presence of weaker interchain interactions in **3** in comparison to **4**. Indeed the pairs of chains shown in Figures 3a and 3b are much more closely packed in the crystal structure of **4** than in **3** as further illustrated by Figures 3c and 3d.

Complexes 5 and 6. Compounds **5** and **6** are extremely unstable in terms of very rapidly losing their interstitial solvent molecules leading to an unknown amorphous material. Therefore, these compounds were studied on polycrystalline samples kept in their mother liquor to avoid any desolvatation or degradation. The temperature dependence of the magnetic susceptibility at 1000 Oe for the two compounds is shown in Figure 9 as an χT vs *T* plot. For both compounds, the χT
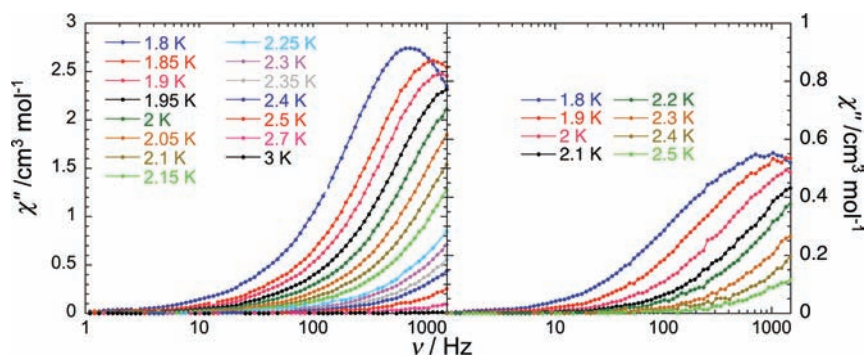

Figure 9. Temperature dependence of the χT product at 1000 Oe for **5** (circles) and **6** (triangles). Solid red and blue lines indicate the best fits obtained with the models described in the text. Inset: ln($\chi'T$) vs 1/*T* plot (χ' being the in-phase ac susceptibility at 1 Hz, 3 Oe of ac field modulation in zero dc field) measured on a polycrystalline sample of **5** (circles) and **6** (triangles). The solid line represents the best fit described in the text.

product at 1000 Oe increases from room temperature (4.1 and 3.9 cm³ K mol⁻¹ for **5** and **6**, respectively) down to 1.8 K (9.9 cm³ K mol⁻¹) for **5** and 15 K (4.2 cm³ K mol⁻¹) for **6**. For this latter compound, the χT value sharply decreases below 15 K down to 2.8 cm³ K mol⁻¹ at 1.8 K.

In contrast to complexes **1−4**, these thermal behaviors suggest the presence of dominant ferromagnetic interactions between Mn(III) and Fe(III) spin carriers through the CN bridges within these chains. The *M* vs *H* data shown in Supporting Information, Figure S12 confirm the ferromagnetic nature of the couplings within the chain as (i) the *M* vs *H* curves do not exhibit an inflection point and (ii) under 7 T at 1.8 K, the magnetization is not saturated, reaching 5.2 and 4.6 μ_B for **5** and **6**, respectively, in good agreement with a ferromagnetic arrangement of the S_{Mn} = 2 Mn(III) and s_{Fe} = 1/2 Fe(III) spins along the chain (ferromagnetic intrachain interaction should lead to a saturated magnetization around 5 μ_B).

The experimental data of **5** and **6** have been modeled using an isotropic Heisenberg Hamiltonian (eq 4, with $S_{Mn,i} = S_{Mn,i+1}$ = 2 and $s_{Fe,i}$ = 1/2) based on the Seiden model for chains of quantum spins *s* = 1/2 and classical *S* = 2 spins.[33] For **6**,

Figure 10. Frequency dependence of the imaginary (χ'') parts of the ac susceptibility for a polycrystalline sample of **5** (left) and **6** (right) in zero dc-field at different temperatures. The solid lines are guides for the eye.

interchain interactions were introduced in the mean-field approximation[31] to reproduce the data below 15 K while that was not necessary for **5**. The experimental data are well reproduced by this model with the following set of parameters: $J/k_B = +1.5(1)$ K and $g = 2.19(5)$ for **5** and $J/k_B = +5.5(3)$ K, $zJ'/k_B = -0.8(4)$ K and $g = 2.1$ (fixed) for **6**. Regarding the ferromagnetic nature of the intrachain magnetic interactions (J) in **5** and **6**, other Fe(III)−CN−Mn(III) systems exhibiting similar properties have been reported.[15c,35]

The investigation of the dynamic properties of **5** and **6** were performed by ac susceptibility measurements on polycrystalline samples maintained in solution between 3 and 1.8 K at zero dc field.
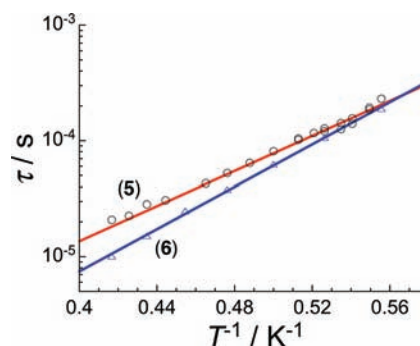
The real (χ') and imaginary (χ'') components of the ac susceptibility have been measured as a function of the temperature above 1.8 K as well as a function of the ac field frequency from 1 to 1500 Hz and are displayed in Figure 10, Supporting Information, Figures S13 and S14. While for all the other compounds reported in this work, the absence of out-of-phase ac susceptibility was systematically confirmed, **5** and **6** show a strong ac susceptibility response below 3 K with a significant frequency dependence of both in-phase and out-of-phase components. This dynamic behavior is the typical signature of SMM or SCM systems that display slow relaxation of their magnetization in the absence of a 3D magnetic order seen in classical magnets. As shown by the analysis of the crystal structures for **5** and **6**, these compounds are 1D coordination polymers that are relatively well separated by chloroform for **5** or methanol/water molecules for **6** (Figures 4). From a magnetic point of view, the 1D nature of **5** and **6** can also be checked following the 1D correlation length, ξ, which is proportional to the χT product at zero field in any 1D classical system. In the particular case of anisotropic Heisenberg or Ising-like 1D behavior, ξ and χT increases exponentially with decreasing temperature

$$\chi T = C_{\mathrm{eff}} \exp(\Delta_\xi / k_B T) \tag{7}$$

where C_{eff} is the effective Curie constant and Δ_ξ is the correlation energy, that is, the energy needed to create a domain wall along the chain. Confirming the 1D magnetic properties of **5**, the experimental $\ln(\chi'T)$ versus $1/T$ data show a exponential increase of the correlation length between 20 and 2 K (Figure 9) with $\Delta_\xi/k_B \approx 2$ K and $C_{\mathrm{eff}} = 4.6$ cm^3 K mol^{-1}. In contrast, $\ln(\chi'T)$ decreases as a function of $1/T$ for **6** as a result of significant interchain antiferromagnetic interactions (vide supra, $zJ'/k_B = -0.8(4)$ K). Therefore an accurate estimation of the 1D energy gap (Δ_ξ) induced by the intrachain

ferromagnetic interactions is made impossible. This result highlights the important role of the interchain couplings and how they can influence the estimation of Δ_ξ especially in presence of weak intrachain magnetic interactions. For **5**, the theoretical Δ_ξ in the Ising limit, $\Delta_\xi = 4|J|S_{\mathrm{Mn}}s_{\mathrm{Fe}}\cos(\theta)$,[36,37] is expected to be equal to about 5.8 K (as $J/k_B = +1.5$ K and $\theta \approx 15°$; θ is the canting angle between local Mn(III) and Fe(III) easy axes, i.e., axial directions) but the experimental energy gap was evaluated only at 2 K most likely because of the weak interchain antiferromagnetic interactions (Figure 4).

On the basis of the ac susceptibility data shown in Figure 10, the temperature dependence of the relaxation time (τ) for **5** and **6** has been determined experimentally (from the maxima of the $\chi''(\nu)$ curves at a given temperature for which $\tau = 1/(2\pi\nu_{\mathrm{max}})$ and from a classical scaling method[38] when the maxima of the $\chi''(\nu)$ curves is not observed experimentally). The obtained τ vs $1/T$ plots are displayed in Figure 11.

Figure 11. Magnetization relaxation time (τ) versus T^{-1} plot for **5** (dots) and **6** (triangles) in zero dc-field. Solid lines are the best fits of the experimental data to the Arrhenius laws discussed in the text.

The experimental relaxation time of these two systems follows an Arrhenius law:

$$\tau = \tau_0 \exp(\Delta_\tau / k_B T) \tag{8}$$

(where τ_0 is a pre-exponential factor, Δ_τ is the energy barrier to reverse the magnetization direction) with $\tau_0 = 1.3 \times 10^{-8}$ s and $\Delta_\tau/k_B = 17$ K for **5** and $\tau_0 = 1.7 \times 10^{-9}$ s and $\Delta_\tau/k_B = 21$ K for **6**. The values of τ_0 that give a quantitative estimation of the attempt time of relaxation from the chain bath are in good agreement with other reported SCM compounds.[12,20c,d,39] As shown in Figure 9 inset and Figure 11, the relaxation time has been evaluated in the temperature region for which the correlations still increase (at least for **5**) and thus in the infinite

chain regime of the relaxation for SCMs.[36] In this regime, the overall spin-reversal barrier can always be expressed as $\Delta_\tau = 2\Delta_\xi + \Delta_A$ with Δ_A being the activation energy barrier arising from the magnetic anisotropy (D) of the system and defined by $\Delta_A = |D|S^2$ in a simple uniaxial anisotropy symmetry with

$$H = DS_z^2 \qquad (9)$$

Having experimentally determined both Δ_τ and Δ_ξ for **5**, Δ_A can be estimated around 13 K. In these systems, as the main contribution to the anisotropy comes from the single-ion anisotropy of Mn(III) ions, it is possible to evaluate the $|D|$ parameter for the Mn(III) metal ion from Δ_A at about 3.2 K. This value is in excellent agreement with estimations between −5 and −2.5 K reported in the literature.[13,20c,26b,36,39,40] For **6**, the discussion of the energy gaps is unfortunately not possible without an experimental estimation of Δ_ξ.

In summary, both complexes **5** and **6** display SCM behavior that was confirmed by both static and dynamic magnetic properties. It should be highlighted that the spin canting angle between Mn(III) and Fe(III) axial directions in these two systems possesses the lowest values ($\theta = 15.3$ and $15.4°$ for **5** and **6**, respectively) among all compounds reported in this work. Manifestly, this structural feature is certainly favoring intrachain ferromagnetic interactions, good alignment of the anisotropy tensors, and thus their SCM behaviors.

Complex 7. The temperature dependence of the χT product shown in Figure 12 was measured at 1000 Oe on a
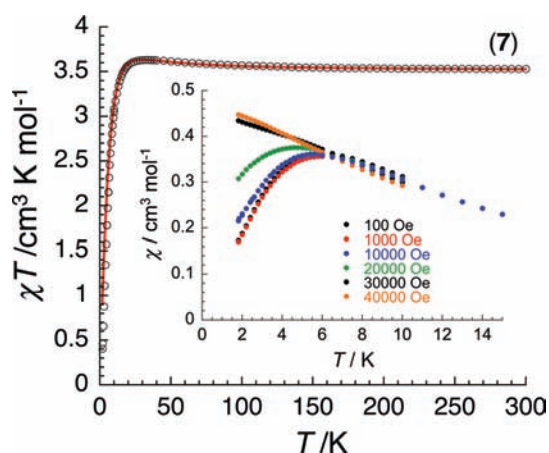

Figure 12. Temperature dependence of the χT product at 1000 Oe for **7**. Solid red line indicates the best fit obtained with the model described in the text. Inset: χ vs T plot between 15 and 1.8 K measured on a polycrystalline sample of **7** at different applied dc magnetic field.

polycrystalline sample of **7**. Upon cooling, the χT product gradually increases from 3.5 cm^3 K mol^{-1} at 300 K to reach a maximum value of 3.65 cm^3 K mol^{-1} at 33 K before a rapid decrease at lower temperatures (0.4 cm^3 K mol^{-1} at 1.8 K). The observed thermal behavior reveals the ferromagnetic nature of the Mn···Fe interactions as already observed in **5** and **6** and also in some Fe(III)−CN−Mn(III) systems built from the [Fe(bpb)(CN)$_2$]$^-$ precursor.[15c,35,41] The experimental data have been modeled using the same spin Hamiltonian as for compounds **5** and **6** (eq 4), thus applying the 1D Seiden approach[33] and treating the interchain interactions in the mean field approximation.[31] The best least-squares fit, shown in Figure 12, yields the following set of parameters: $J/k_B = +6.7(2)$

K, $zJ'/k_B = -1.5(2)$ K, and $g = 2.0$ fixed. The ferromagnetic interaction between Fe(III) and Mn(III) magnetic centers is also confirmed by the field dependence of the magnetization below 10 K (Supporting Information, Figure S15). Even at 1.8 K under 7 T, the magnetization does not saturate but reaches 4.2 μ_B in good agreement with the saturation value of 5 μ_B expected for ferromagnetically coupled Mn(III) ($S = 2$) and one Fe(III) ($s_{Fe} = 1/2$) spins.

Like for **3** and **4** (vide supra), the magnetic susceptibility of **7** becomes strongly field dependent below 6 K as shown in Figure 12 inset. This behavior is also seen in the M vs H data (Supporting Information, Figure S15), which exhibit an inflection point between 6 and 1.8 K emphasized by the maximum of the dM/dH vs H plots (Supporting Information, Figure S15). The observed low temperature properties are clearly the result of antiferromagnetic interchain interactions already detected in modeling the χT vs T data ($zJ'/k_B = -1.5(2)$ K). Therefore, to determine the presence or absence of a 3D antiferromagnetic ground state, the H vs T magnetic phase diagram has been built. Combining M vs H and χ vs T data and taking the maximum of the dM/dH vs H and χ vs T plots (Figure 12 and Supporting Information, Figure S15), the temperature dependence of H_c (Figure 13) was followed from
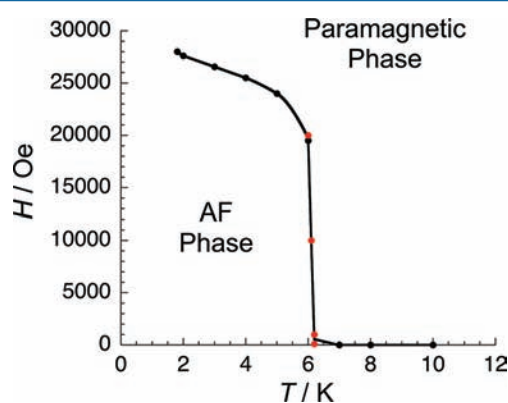
Figure 13. H vs T magnetic phase diagram for **7**. The black and red dots are respectively the experimental points deduced from the M vs H and χ vs T data (Figure 12 and Supporting Information, Figure S15). The solid black line is a guide for the eye.

28000 Oe at 1.8 K until it vanished around 6.1 K (T_N) proving the presence of an antiferromagnetic ground state in **7**. As previously done for **3** and **4**, the interchain interactions can be evaluated at about −1.3 K from the H_c value by applying eq 5. This result is in excellent agreement with the value ($zJ'/k_B = -1.5(2)$ K) determined from the fit of the χT vs T data at 1000 Oe (Figure 12) and also with the estimations done for **3**, **4**, and **6**.

■ CONCLUDING REMARKS

In this work, we have described the preparation and characterization of a new series of materials based on the [Mn(III)−CN−Fe(III)] dinuclear motif. The association of [Fe(L)(CN)$_3$]$^-$ and [Fe(L)(CN)$_2$]$^-$ anionic precursors with anisotropic Mn(III) Schiff-base cations leads to different structural arrangements including two discrete dinuclear complexes (**1** and **2**) and five 1D coordination polymers (**3**−**7**). Hydrogen bonds, short contacts and weak π−π interactions cause the formation of 2D or 3D supramolecular architectures that strongly influence the magnetic ground state of these

systems (diamagnetic for **1**, **2**, paramagnetic for **5** and **6**, and antiferromagnetic for **3**, **4**, and **7** based on experimental data down to 1.8 K). The nature of the Mn(III)···Fe(III) magnetic interactions mediated by the cyanido bridge have been determined by magnetic susceptibility measurements. Like in *mer*-Fe tricyanido-bridged complexes[18c−e,42] and a few recent examples,[29] significant antiferromagnetic interactions are detected in **1−4** between the low-spin s = 1/2 Fe(III) and high-spin S = 2 Mn(III) centers. On the other hand, like in a majority of related compounds,[15c,35,41,42] ferromagnetic interactions are present in **5−7**. As demonstrated by Yoo et al.,[29b] the nature and magnitude of the Mn(III)···Fe(III) magnetic interactions through the CN bridge is influenced by a subtle convolution of geometrical parameters that govern magnetic orbital overlaps. Unfortunately, the magnetic interaction is a simple function of neither the Mn−N_{ax}−C_{ax} angle nor the Mn−N_{ax} bond length nor the torsion angles of C_{eq}−Fe−Mn−$N(O)_{eq}$ but together these structural variables induce the antiferromagnetic or ferromagnetic interaction in the Fe(III)−CN−Mn(III) motif. Therefore, it has been impossible so far to establish a clear magneto-structural correlation in this type of systems that include all the reported results.

At low temperatures, dinuclear S_T = 3/2 [Fe(L)(CN)$_3$Mn-("salen")] complexes in **1** interact antiferromagnetically in their 3D crystal structure while they form supramolecular diamagnetic pairs in **2**. For the 1D systems, interchain antiferromagnetic interactions induce in **3**, **4** and **7** a 3D antiferromagnetic ordered ground state with a metamagnetic behavior as established by the experimental (T, H) magnetic phase diagrams. In the case of **5** and **6**, they both exhibit SCM properties even in the presence of significant interchain antiferromagnetic interactions in **6**. So far these two 1D materials are the only examples of fully characterized SCMs with a Mn(III)−NC−(L)Fe(III)−CN repeating chain motif although some reported materials, like [Fe(qcq)(CN)$_3$][Mn(salen)]·CH$_3$CN·H$_2$O,[18e] [Fe(pzcq)(CN)$_3$][Mn(salen)]·4H$_2$O,[18b] or [Fe(bpb)(CN)$_2$][Mn(5-Me-salen)]·0.5H$_2$O·MeOH,[15c] display slow relaxation of the magnetization without experimental proof of their 1D correlations and thus their SCM behavior.

■ ASSOCIATED CONTENT

Ⓢ Supporting Information

X-ray crystallographic files in CIF format for **1−7**, additional structural and magnetic data. This material is available free of charge via the Internet at http://pubs.acs.org.

■ AUTHOR INFORMATION

Corresponding Author

*E-mail: clerac@crpp-bordeaux.cnrs.fr (R.C.), pichon@crpp-bordeaux.cnrs.fr (C.P.).

Notes

The authors declare no competing financial interest.

■ ACKNOWLEDGMENTS

■ REFERENCES

(1) See for example: (a) Yaghi, O. M.; Li, G.; Li, H. *Nature* **1995**, *378*, 703. (b) *Molecular Magnetism: From the Molecular Assemblies to the Devices*; Coronado, E., Delhaès, P., Gatteschi, D., Miller, J. S., Eds.; NATO ASI Series C484; Kluwer Academic Publishers: Dordrecht, The Netherlands, 1996; pp 43 and 179. (c) Li, H.; Eddaoui, M.; O'Keeffe, M.; Yaghi, O. M. *Nature* **1999**, *402*, 276. (d) Coronado, E.; Galán-Mascarós, J. R.; Gómez-García, C. J.; Laukhin, V. *Nature* **2000**, *408*, 447. (e) Janiak, C. *Dalton Trans.* **2003**, 2781. (f) Beltran, L. M. C.; Long, J. R. *Acc. Chem. Rev.* **2005**, *38*, 325 and references within. (g) Lee, J.; Farha, O. K.; Roberts, J.; Scheidt, K. A.; Nguyen, S. T.; Hupp, J. T. *Chem. Soc. Rev.* **2009**, *38*, 1450.

(2) See for example: (a) Miyasaka, H.; Matsumoto, N.; Okawa, H.; Re, N.; Gallo, E.; Floriani, C. *J. Am. Chem. Soc.* **1996**, *118*, 981 and references within. (b) Miyasaka, H.; Matsumoto, N.; Re, N.; Gallo, E.; Floriani, C. *Inorg. Chem.* **1997**, *36*, 670. (c) Shores, M. P.; Sokol, J. J.; Long, J. R. *J. Am. Chem. Soc.* **2002**, *124*, 2279. (d) Li, D.-F.; Gao, S.; Zheng, L.-M.; Tang, W.-X. *J. Chem. Soc., Dalton Trans.* **2002**, 2805. (e) Bennett, M. V.; Long, J. R. *J. Am. Chem. Soc.* **2003**, *125*, 2394. (f) Pradhan, R.; Desplanches, C.; Guionneau, P.; Sutter, J.-P. *Inorg. Chem.* **2003**, *42*, 6607. (g) Kashiwagi, T.; Ohkoshi, S.-I.; Seino, H.; Mizobe, Y.; Hashimoto, K. *J. Am. Chem. Soc.* **2004**, *126*, 5024. (h) Ruiz, E.; Rodríguez-Fortea, A.; Alvarez, S.; Verdaguer, M. *Chem.—Eur. J.* **2005**, *11*, 2135. (i) Podgajny, R.; Balanda, M.; Sikora, M.; Borowiec, M.; Spalek, L.; Kapusta, C.; Sieklucka, B. *Dalton Trans.* **2006**, 2801. (j) Visinescu, D.; Desplanches, C.; Imaz, I.; Bahers, V.; Pradhan, R.; Villamena, F. A.; Guionneau, P.; Sutter, J.-P. *J. Am. Chem. Soc.* **2006**, *128*, 10202. (k) Lim, J. H.; Yoon, J. H.; Kim, H. C.; Hong, C. S. *Angew. Chem., Int. Ed.* **2006**, *45*, 7424. (l) Miyasaka, H.; Saitoh, A.; Abe, S. *Coord. Chem. Rev.* **2007**, *251*, 2622. (m) Withers, J. R.; Li, D.; Jeremy, T.; Ruschman, C.; Parkin, S.; Wang, G.; Yee, G. T.; Holmes, S. M. *Polyhedron* **2007**, *26*, 2353. (n) Funck, K. E.; Hilfiger, M. G.; Berlinguette, C. P.; Shatruk, M.; Wernsdorfer, W.; Dunbar, K. R. *Inorg. Chem.* **2009**, *48*, 3438. (o) Kosaka, W.; Imoto, K.; Tsunobuchi, Y.; Ohkoshi, S.-i. *Inorg. Chem.* **2009**, *48*, 4604. (p) Freiherr von Richthofen, C.-G.; Stammler, A.; Bögge, H.; DeGroot, M. W.; Long, J. R.; Glaser, T. *Inorg. Chem.* **2009**, *48*, 10165. (q) Shatruk, M.; Avendano, C.; Dunbar, K. R. *Prog. Inorg. Chem.* **2009**, *56*, 155.

(3) Verdaguer, M.; Bleuzen, A.; Marvaud, V.; Vaissermann, J.; Seuleiman, M.; Desplanches, C.; Scuiller, A.; Train, C.; Garde, R.; Gelly, G.; Lomenech, C.; Rosenman, I.; Veillet, P.; Cartier dit Moulin, C.; Villain, F. *Coord. Chem. Rev.* **1999**, *192*, 1023 and references within.

(4) See for example: (a) Lescouëzec, R.; Vaisserman, J.; Ruiz-Pérez, C.; Lloret, F.; Carrasco, R.; Julve, M.; Verdaguer, M.; Dromzee, Y.; Gatteschi, D.; Wernsdorfer, W. *Angew. Chem., Int. Ed.* **2003**, *42*, 1483. (b) Darensbourg, D. J.; Phelps, A. L. *Inorg. Chim. Acta* **2004**, *357*, 1603. (c) Toma, L.; Lescouëzec, R.; Vaissermann, J.; Delgado, F. S.; Ruiz-Pérez, C.; Carrasco, R.; Cano, J.; Lloret, F.; Julve, M. *Chem.—Eur. J.* **2004**, *10*, 6130. (d) Kim, J.; Cho, I. K.; Choi, K. Y.; Heu, M.; Yoon, S.; Suh, B. J. *Polyhedron* **2004**, *23*, 1333. (e) Zhang, Y.-Z.; Gao, S.; Wang, Z.-M.; Su, G.; Sun, H.-L.; Pan, F. *Inorg. Chem.* **2005**, *44*, 4534. (f) Visinescu, D.; Fabelo, O.; Ruiz-Pérez; Lloret, F.; Julve, M. *CrystEngComm.* **2010**, *12*, 2454. (g) Nastase, S.; Maxim, C.; Andruh, M.; Cano, J.; Ruiz-Pérez, C.; Faus, J.; Lloret, F.; Julve, M. *Dalton Trans.* **2011**, *40*, 4898.

(5) (a) Yang, J. Y.; Shores, M. P.; Sokol, J. J.; Long, J. R. *Inorg. Chem.* **2003**, *42*, 1403. (b) Wang, S.; Zuo, J. L.; Zhou, H. C.; Choi, H. J.; Ke, Y.; Long, J. R.; You, X. Z. *Angew. Chem., Int. Ed.* **2004**, *43*, 5940. (c) Schelter, E. J.; Prosvirin, A. V.; Reiff, W. M.; Dunbar, K. R. *Angew. Chem., Int. Ed.* **2004**, *43*, 4912. (d) Li, D.; Parkin, S.; Wang, G.; Yee, G. T.; Clérac, R.; Wernsdorfer, W.; Holmes, S. M. *J. Am. Chem. Soc.* **2006**, *128*, 4214. (e) Schelter, E. J.; Karadas, F.; Avendano, C.; Prosvirin, A. V.; Wernsdorfer, W.; Dunbar, K. R. *J. Am. Chem. Soc.* **2007**, *129*, 8139.

(f) Wang, C. F.; Liu, W.; Song, Y.; Zhou, X.-H.; Zuo, J.-L.; You, X. Z. *Eur. J. Inorg. Chem.* **2008**, 717. (g) Li, D.; Clérac, R; Roubeau, O.; Harté, E.; Mathonière, C.; Le Bris, R.; Holmes, S. M. *J. Am. Chem. Soc.* **2008**, *130*, 252. (h) Karadas, F.; Avendano, C.; Hilfiger, M. G.; Prosvirin, A. V.; Dunbar, K. R. *Dalton Trans.* **2010**, 4968.

(6) (a) Darensbourg, D. J.; Lee, W.-Z.; Adams, M. J.; Larkins, D. L.; Reibenspies, J. H. *Inorg. Chem.* **1999**, *38*, 1378. (b) Oshio, H.; Tamada, O.; Onodera, H.; Ito, T.; Ikoma, T.; Tero-Kubota, S. *Inorg. Chem.* **1999**, *38*, 5686. (c) Oshio, H.; Onodera, H.; Tamada, O.; Mizutani, H.; Hikichi, H.; Ito, T. *Chem.—Eur. J.* **2000**, *6*, 2523. (d) Oshio, H.; Yamamoto, M.; Ito, T. *Inorg. Chem.* **2002**, *41*, 5817. (e) Li, D.; Parkin, S.; Wang, G.; Yee, G. T.; Prosvirin, A. V.; Holmes, S. M. *Inorg. Chem.* **2005**, *44*, 4903. (f) Jiang, L.; Lu, T. B.; Feng, X.-L. *Inorg. Chem.* **2005**, *44*, 7056. (g) Li, D.; Parkin, S.; Wang, G.; Yee, G. T.; Holmes, S. M. *Inorg. Chem.* **2006**, *45*, 1951. (h) Rodríguez-Diéguez, A.; Kivekäs, R.; Sillanpää, R.; Cano, J.; Lloret, F.; McKee, V.; Stoeckli-Evans, H.; Colacio, E. *Inorg. Chem.* **2006**, *45*, 10537. (i) Li, D.; Clérac, R.; Wang, G.; Yee, G. T.; Holmes, S. M. *Eur. J. Inorg. Chem.* **2007**, 1341. (j) Karadas, F.; Schelter, E. J.; Schatruk, M.; Prosvirin, A. V.; Bacsa, J.; Smirnov, D.; Ozarowski, A.; Krzystek, J.; Telser, J.; Dunbar, K. R. *Inorg. Chem.* **2008**, *47*, 2074. (k) Vreshch, O. V.; Nesterova, O. V.; Kokozay, V. N.; Skelton, B. W.; Gómez Gárcia, C. J.; Jezierska, J. *Inorg. Chem. Commun.* **2009**, *12*, 890. (l) Wu, D.-Y.; Sato, O.; Duan, C.-Y. *Inorg. Chem. Commun.* **2009**, *12*, 325. (m) Halbauer, K.; Spielberg, E. T.; Sterzik, A.; Plass, W.; Imhof, W. *Inorg. Chim. Acta* **2010**, *363*, 1013. (n) Karadas, F.; Shatruk, M.; Perez, L. M.; Dunbar, K. R. *Chem.—Eur. J.* **2010**, *16*, 7164. (o) Zhang, Y.; Li, D.; Clérac, R.; Kalisz, M.; Mathonière, C.; Holmes, S. M. *Angew. Chem., Int. Ed.* **2010**, *49*, 3752. (p) Wu, D.; Zhang, Y.; Huang, W.; Sato, O. *Dalton Trans.* **2010**, *39*, 5500. (q) Galstyan, A.; Sanz Miguel, P. J.; Wolf, J.; Freisinger, E.; Lippert, B. *Eur. J. Inorg. Chem.* **2011**, 1649. (r) Nihei, M.; Sekine, Y.; Suganami, N.; Nakazawa, K.; Nakao, A.; Nakao, H.; Murakami, Y.; Oshio, H. *J. Am. Chem. Soc.* **2011**, *133*, 3592. (s) Siretanu, D.; Li, D.; Buisson, L.; Bassani, D. M.; Holmes, S. M.; Mathonière, C.; Clérac, R. *Chem.—Eur. J.* **2011**, *17*, 11704. (t) Pardo, E.; Verdaguer, M.; Herson, P.; Rousselière, H.; Cano, H.; Julve, M.; Lloret, F.; Lescoüezec, R. *Inorg. Chem.* **2011**, *50*, 6250. (u) Newton, G. N.; Nihei, M.; Oshio, H. *Eur. J. Inorg. Chem.* **2011**, 3031. (v) Kang, L.-C.; Yao, M.-X.; Chen, X.; Li, Y.-Z.; Song, Y.; Zuo, J.-L.; You, X.-Z. *Dalton Trans.* **2011**, *40*, 2204.

(7) See for example: (a) Colacio, E.; Domínguez-Vera, J. M.; Lloret, F.; Moreno Sánchez, J. M.; Kivekaäs, R.; Rodríguez, A.; Sillanpää. *Inorg. Chem.* **2003**, *42*, 4209. (b) Figuerola, A.; Ribas, J.; Solans, X.; Font-Bardía, M.; Maestro, M.; Diaz, C. *Eur. J. Inorg. Chem.* **2006**, 846. (c) Zhang, Y. Z.; Duan, G. P.; Sato, O.; Gao, S. *J. Mater. Chem.* **2006**, *16*, 2625. (d) Coronado, E.; Gómez-García, C. J.; Nuez, A.; Romero, F. M.; Waerenborgh, J. C. *Chem. Mater.* **2006**, *18*, 2670. (e) Gu, Z.-G.; Yang, Q.-F.; Zuo, J.-L.; Zeng, X. R.; Zhou, H.-C.; You, X.-Z. *Inorg. Chim. Acta* **2006**, *359*, 3790. (f) Liu, X.; Roubeau, O.; Clérac, R. *C. R. Chim.* **2008**, *11*, 1182. (g) Costa, V.; Lescoüezec, R.; Vaissermann, J.; Herson, P.; Journaux, Y.; Araujo, M. H.; Clemente-Juan, J. M.; Lloret, F.; Julve, M. *Inorg. Chim. Acta* **2008**, *361*, 3912. (h) Gheorghe, R.; Kalisz, M.; Clérac, R.; Mathonière, C.; Herson, P.; Li, Y.; Seuleiman, M.; Lescoüezec, R.; Lloret, F.; Julve, M. *Inorg. Chem.* **2010**, *49*, 11045. (i) Nowicka, B.; Balanda, M.; Gawel, B.; Ćwiak, G.; Budziak, A.; Łasocha, W.; Sieklucka, B. *Dalton Trans.* **2011**, *40*, 3067.

(8) (a) Berlinguette, C. P.; Vaughn, D.; Canada-Vilalta, C.; Galan-Mascaros, J.-R.; Dunbar, K. R. *Angew. Chem., Int. Ed.* **2003**, *42*, 1523. (b) Sokol, J. J.; Hee, A. G.; Long, J. R. *J. Am. Chem. Soc.* **2002**, *124*, 7656. (c) Choi, H. J.; Sokol, J. J.; Long, J. R. *Inorg. Chem.* **2004**, *43*, 1606. (d) Schelter, E. J.; Prosvirin, A. V.; Dunbar, K. R. *J. Am. Chem. Soc.* **2004**, *126*, 15004. (e) Miyasaka, H.; Takahashi, H.; Madanbashi, T.; Sugiura, K.; Clérac, R.; Nojiri, H. *Inorg. Chem.* **2005**, *44*, 5969. (f) Li, D.; Clérac, R.; Parkin, S.; Wang, G.; Yee, G. T.; Holmes, S. M. *Inorg. Chem.* **2006**, *45*, 5251. (g) Wang, C.-F.; Zuo, J.-L.; Bartlett, B. M.; Song, Y.; Long, J. R.; You, X.-Z. *J. Am. Chem. Soc.* **2006**, *128*, 7162. (h) Yoon, J. H.; Kim, H. C.; Hong, C. S. *Inorg. Chem.* **2006**, *45*, 9613. (i) Rebilly, J.-N.; Mallah, T. *Struct. Bonding (Berlin)* **2006**, *122*, 103. (j) Freedman, D. E.; Bennett, M. V.; Long, J. R. *Dalton Trans.* **2006**, 2829. (k) Jiang, L.; Choi, H. J.; Feng, X.-L.; Lu, T.-B.; Long, J.-R. *Inorg.*

Chem. **2007**, *46*, 2181. (l) Ni, Z. H.; Zhang, L.-F.; Tangoulis, V.; Wernsdorfer, W.; Cui, A.-L.; Sato, O.; Kou, H.-Z. *Inorg. Chem.* **2007**, *46*, 6029. (m) Zhang, Y.; Mallik, U. P.; Rath, N.; Yee, G. T.; Clérac, R.; Holmes, S. M. *Chem. Commun.* **2010**, *46*, 4953. (n) Pedersen, K. S.; Schau-Magnussen, M.; Bendix, J.; Weihe, H.; Palii, A. V.; Klokishner, S. I.; Ostrovsky, S.; Reu, O. S.; Mutka, H.; Tregenna-Piggott, P. L. W. *Chem.—Eur. J.* **2010**, *16*, 13458. (o) Wang, X.-Y.; Avendaño, C.; Dunbar, K. R. *Chem. Soc. Rev.* **2011**, *40*, 3213. (p) Harris, T. D.; Soo, H. S.; Chang, C. J.; Long, J. R. *Inorg. Chim. Acta* **2011**, *369*, 91.

(9) (a) Wang, S.; Zuo, J. L.; Gao, S.; Song, Y.; Zhou, H. C.; Zhang, Y. Z.; You, X. Z. *J. Am. Chem. Soc.* **2004**, *126*, 8900. (b) Lescoüezec, R.; Toma, L. M.; Vaissermann, J.; Verdaguer, M.; Delgado, F. S.; Ruiz-Pérez, C.; Lloret, F.; Julve, M. *Coord. Chem. Rev.* **2005**, *249*, 2691 and references within. (c) Toma, L. M.; Lescoüezec, R.; Pasán, J.; Ruiz-Pérez, C.; Vaissermann, J.; Cano, J.; Carrasco, R.; Wernsdorfer, W.; Lloret, F.; Julve, M. *J. Am. Chem. Soc.* **2006**, *128*, 4842. (d) Miyasaka, H.; Julve, M.; Yamashita, M.; Clérac, R. *Inorg. Chem.* **2009**, *48*, 3420. (e) Hoshino, N.; Sekine, Y.; Nihei, M.; Oshio, H. *Chem. Commun.* **2010**, *46*, 6117. (f) Harris, T. D.; Bennett, M. V.; Clérac, R.; Long, J. R. *J. Am. Chem. Soc.* **2010**, *132*, 3980. (g) Zhang, D.; Zhang, L.-F.; Chen, Y.; Wang, H.; Ni, Z.-H.; Wernsdorfer, W.; Jiang, J. *Chem. Commun.* **2010**, *46*, 3550.

(10) (a) Leuenberger, M. N.; Loss, D. *Nature* **2001**, *410*, 789. (b) Wernsdorfer, W.; Aliaga-Alcalde, N.; Hendrickson, D. N.; Christou, G. *Nature* **2002**, *416*, 406. (d) Gatteschi, D.; Sessoli, R. *Angew. Chem., Int. Ed.* **2003**, *42*, 268. (e) Troiani, F.; Ghirri, A.; Affronte, M.; Carretta, S.; Santini, P.; Amoretti, G.; Piligkos, S.; Timco, G.; Winpenny, R. E. P. *Phys. Rev. Lett.* **2005**, *94*, 207208. (f) Troiani, F.; Affronte, M.; Carretta, S.; Santini, P.; Amoretti, G. *Phys. Rev. Lett.* **2005**, *94*, 190501. (g) Gatteschi, D.; Sessoli, R.; Villain, J. *Molecular Nanomagnets*; Oxford University Press: New York, 2006, and references within (h) Lehmann, J.; Gaita-Arino, A.; Coronado, E.; Loss, D. *Nat. Nanotechnol.* **2007**, *2*, 312. (i) Bogani, L.; Wernsdorfer, W. *Nat. Mater.* **2008**, *7*, 179. (j) Stepanenko, D.; Trif, M.; Loss, D. *Inorg. Chim. Acta* **2008**, *361*, 3740. (c) Long, J. R.; Yang, P. *Chemistry of Nanostructured Materials* **2003**, 291−315 and references within.

(11) Ferbinteanu, M.; Miyasaka, H.; Wernsdorfer, W.; Nakata, K.; Sugiura, K.−I.; Yamashita, M.; Coulon, C.; Clérac, R. *J. Am. Chem. Soc.* **2005**, *127*, 3090.

(12) Miyasaka, H.; Madanbashi, T.; Saitoh, A.; Motokawa, N.; Ishikawa, R.; Yamashita, M.; Bahr, S.; Wernsdorfer, W.; Clérac, R. *Chem.—Eur. J.* **2012**, DOI: 10.1002/chem201102738.

(13) Miyasaka, H.; Clérac, R.; Wernsdorfer, W.; Lecren, L.; Bonhomme, C.; Sugiura, K.; Yamashita, M. *Angew. Chem., Int. Ed.* **2004**, *43*, 2801.

(14) (a) Lescoüezec, R.; Vaissermann, J.; Toma, L. M.; Carrasco, R.; Lloret, F.; Julve, M. *Inorg. Chem.* **2004**, *43*, 2234. (b) Kwak, H. Y.; Ryu, D. W.; Lee, J. W.; Yoon, J. H.; Kim, H. C.; Koh, E. K.; Krinsky, J.; Hong, C. S. *Inorg. Chem.* **2010**, *49*, 4632.

(15) (a) Ni, Z.-H.; Kou, H.-Z.; Zao, Y.-H.; Zheng, L.; Wang, R.-J.; Cui, A.-L.; Sato, O. *Inorg. Chem.* **2005**, *44*, 2050. (b) Ni, Z.-H.; Kou, H.-Z.; Zheng, L.; Zhao, Y.-H.; Zhang, L.-F.; Wang, R.-J.; Cui, A.-L.; Sato, O. *Inorg. Chem.* **2005**, *44*, 4728. (c) Kou, H.-Z.; Ni, Z.-H.; Liu, C.-M.; Zhang, D.-Q.; Cui, A.-L. *New J. Chem.* **2009**, *33*, 2296. (d) Zhang, D.; Wang, H.; Chen, Y.; Ni, Z.-H.; Tian, L.; Jiang, J. *Inorg. Chem.* **2009**, *48*, 5488. (e) Ni, Z.-H.; Tao, J.; Wernsdorfer, W.; Cui, A.-L.; Kou, H.-Z. *Dalton Trans.* **2009**, *15*, 2788.

(16) Wang, S.; Ding, X.-H.; Zuo, J.-L.; You, X.-Z.; Huang, W. *Coord. Chem. Rev.* **2011**, *255*, 1713 and references within.

(17) (a) Gu, Z.-G.; Yang, Q.-F.; Liu, W.; Song, Y.; Li, T.-Z.; Zuo, J.-L.; You, X.-Z. *Inorg. Chem.* **2006**, *45*, 8895. (b) Liu, W.; Wang, C.-F.; Li, Y.-Z.; Zuo, J.-L.; You, X.-Z. *Inorg. Chem.* **2006**, *45*, 10058. (c) Wen, H.-R.; Wang, C.-F.; Song, Y.; Gao, S.; Zuo, J.-L.; You, X.-Z. *Inorg. Chem.* **2006**, *45*, 8942. (d) Li, X.-M.; Wang, C.-F.; Ji, Y.; Kang, L.-C.; Zhou, X.-H.; Zuo, J.-L.; You, X.-Z. *Inorg. Chem.* **2009**, *48*, 9166. (e) Zhang, Y.-J.; Liu, T.; Kanegawa, S.; Sato, O. *J. Am. Chem. Soc.* **2010**, *132*, 912. (f) Kang, L.-C.; Chen, X.; Wang, H. S.; Li, Y.-Z.; Song, Y.; Zuo, J.-L.; You, X.-Z. *Inorg. Chem.* **2010**, *49*, 9275.

(18) (a) Ni, Z.-H.; Kou, H.-Z.; Zhang, L.-F.; Ni, W.-W.; Jiang, Y.-B.; Cui, A.-L.; Ribas, J.; Sato, O. *Inorg. Chem.* **2005**, *44*, 9631. (b) Kim, J. I.; Yoo, H. S.; Koh, E. K.; Kim, H. C.; Hong, C. S. *Inorg. Chem.* **2007**, *46*, 8481. (c) Kim, J. I.; Yoo, H. S.; Koh, E. K.; Hong, C. S. *Inorg. Chem.* **2007**, *46*, 10461. (d) Kim, J. I.; Yoon, J. H.; Kwak, H. Y.; Koh, E. K.; Hong, C. S. *Eur. J. Inorg. Chem.* **2008**, 2756. (e) Kim, J. I.; Kwak, H. Y.; Yoon, J. H.; Ryu, D. W.; Yoo, I. Y.; Yang, N.; Koh, E. K.; Park, J. G.; Lee, H.; Hong, C. S. *Inorg. Chem.* **2009**, *48*, 2956.

(19) (a) Wocadlo, S.; Massa, W.; Folgado, J. V. *Inorg. Chim. Acta* **1993**, *207*, 199. (b) Kamiyama, A.; Noguchi, T.; Kajiwara, T.; Ito, T. *Inorg. Chem.* **2002**, *41*, 507.

(20) (a) Si, S.-F.; Tang, J.-K.; Liu, Z.-Q.; Liao, D.-Z.; Jiang, Z.-H.; Yan, S.-P.; Cheng, P. *Inorg. Chem. Commun.* **2000**, *6*, 1109. (b) Miyasaka, H.; Clérac, R.; Ishii, T.; Chang, H.-C.; Kitagawa, S.; Yamashita, M. *J. Chem. Soc., Dalton Trans.* **2002**, *7*, 1528 and references within. (c) Miyasaka, H.; Clérac, R.; Mizushima, K.; Sugiura, K.; Yamashita, M.; Wernsdorfer, W.; Coulon, C. *Inorg. Chem.* **2003**, *42*, 8203 and references within. (d) Miyasaka, H.; Nezu, T.; Sugimoto, K.; Sugiura, K.; Yamashita, M.; Clérac, R. *Inorg. Chem.* **2004**, *43*, 5486 and references within.

(21) Wen, H.-R.; Wang, C.-F.; Zuo, J.-L.; Song, Y.; Zeng, X.-R.; You, X.-Z. *Inorg. Chem.* **2006**, *45*, 582.

(22) (a) Ray, M.; Mukherjee, R.; Richardson, J. F.; Buchanan, R. M. *J. Chem. Soc., Dalton Trans.* **1993**, 2451. (b) Dutta, S. K.; Beckmann, U.; Bill, E.; Weyhermuller, T.; Wieghardt, K. *Inorg. Chem.* **2000**, *39*, 3355.

(23) Otwinowski, Z.; Minor, W. *Methods Enzymol.* **1996**, *276*, 307.

(24) (a) *SHELXTL*; Bruker AXS Inc.: Madison, WI. (b) Sheldrick, G. M. *Acta Crystallogr., Sect. A* **2008**, *64*, 112−122.

(25) Shyu, H.-L.; Wei, H.-H.; Wang, Y. *Inorg. Chim. Acta* **1999**, *290*, 8.

(26) (a) Bonadies, B. A.; Kirk, M. L.; Lah, M. S.; Kessissoglou, D. P.; Hatfield, W. E.; Pecoraro, V. L. *Inorg. Chem.* **1989**, *28*, 2037. (b) Miyasaka, H.; Nezu, T.; Sugimoto, K.; Sugiura, K. -I.; Yamashita, M.; Clérac, R. *Chem.—Eur. J.* **2005**, *11*, 1592.

(27) (a) Nakamoto, K. *Infrared and Raman Spectra of Inorganic and Coordination Compounds*, 5th ed.; Wiley: New York, 1997; Part B, pp 105−113. (b) Nakamoto, K. *Infrared and Raman Spectra of Inorganic and Coordination Compounds*, 5th ed.; Wiley: New York, 1997; Part B, p 38. (c) Xiang, J.; Man, W. L.; Guo, J.; Yiu, S. M.; Lee, G.-H.; Peng, S.-M.; Xu, G.; Gao, S.; Lau, T. C. *Chem. Commun.* **2010**, *46*, 6102.

(28) (a) Zhang, D.; Wang, H.; Chen, Y.; Ni, Z.-H.; Tian, L.; Jiang, J. *Inorg. Chem.* **2009**, *48*, 11215. (b) Visinescu, D.; Toma, L. M.; Cano, J.; Fabelo, O.; Ruiz-Pérez, C.; Labrador, A.; Lloret, F.; Julve, M. *Dalton Trans.* **2010**, *39*, 5028.

(29) (a) Wen, H.-R.; Tang, Y.-Z.; Liu, C.-M.; Chen, J.-L.; Yu, C.-L. *Inorg. Chem.* **2009**, *48*, 10177. (b) Yoo, I.-Y.; Ryu, D. W.; Yoon, J. H.; Sohn, A. R.; Lim, K. S.; Cho, B. K.; Koh, E. K.; Hong, C. S. *Dalton Trans.* **2012**, *41*, 1776.

(30) Kajiwara, T.; Ito, T. *Acta Crystallogr.* **2000**, *C56*, 22.

(31) To take into account the interactions between Mn(III) and Fe(III) ions through hydrogen bonds, the following expression of the susceptibility has been used: $\chi = \chi_{MnFe}/\{1 - [(2zJ')/(Ng^2\mu_B^2)]\chi_{MnFe}\}$. See for example: (a) Myers, B. E.; Berger, L.; Friedberg, S. *J. Appl. Phys.* **1969**, *40*, 1149. (b) O'Connor, C. J. *Prog. Inorg. Chem.* **1982**, *29*, 203.

(32) (a) Borrás-Almenar, J. J.; Clemente-Juan, J. M.; Coronado, E.; Tsukerblat, B. S. *Inorg. Chem.* **1999**, *38*, 6081. (b) Borrás-Almenar, J. J.; Clemente-Juan, J. M.; Coronado, E.; Tsukerblat, B. S. *J. Comput. Chem.* **2001**, *22*, 985.

(33) Seiden, J. *J. Phys., Lett.* **1983**, *44*, L947.

(34) (a) Jongh, L. J.; Miedema, A. R. *Adv. Phys.* **1974**, *23*, 1. (b) Chikazumi, S. *Physics of Ferromagnetism*; Clarendon Press, Oxford Science Publication: Oxford, 1997; p 521. (c) Coulon, C.; Clérac, R.; Lecren, L.; Miyasaka, H. *Phys. Rev. B* **2004**, *69*, 132408.

(35) Ni, Z.-H.; Kou, H.-Z.; Zhang, L.-F.; Ge, C.; Cui, A.-L.; Wang, R.-J.; Li, Y.; Sato, O. *Angew. Chem., Int. Ed.* **2005**, *44*, 7742.

(36) Coulon, C.; Miyasaka, H.; Clérac, R. *Struct. Bonding (Berlin)* **2006**, *122*, 163.

(37) Bernot, K.; Luzon, J.; Sessoli, R.; Vindigni, A.; Thion, J.; Richeter, S.; Leclercq, D.; Larionova, J.; van der Lee, A. *J. Am. Chem. Soc.* **2008**, *130*, 1619.

(38) Labarta, A.; Iglesias, O.; Barcells, L. I.; Badia, F. *Phys. Rev. B* **1993**, *48*, 10240.

(39) (a) Clérac, R.; Miyasaka, H.; Yamashita, M.; Coulon, C. *J. Am. Chem. Soc.* **2002**, *124*, 12837. (b) Balanda, M.; Rams, M.; Nayak, S. K.; Tomkowicz, Z.; Haase, W.; Tomala, K.; Yahkmi, J. V. *Phys. Rev. B* **2006**, *74*, 224421. (c) Miyasaka, H.; Madanbashi, T.; Sugimoto, K.; Nakazawa, Y.; Wernsdorfer, W.; Sugiura, K.-i.; Yamashita, M.; Coulon, C.; Clérac, R. *Chem.—Eur. J.* **2006**, *12*, 7028. (d) Lecren, L.; Wernsdorfer, W.; Li, Y.-G.; Vindigni, A.; Miyasaka, H.; Clérac, R. *J. Am. Chem. Soc.* **2007**, *129*, 5045. (e) Miyasaka, H.; Saitoh, A.; Yamashita, M.; Clérac, R. *Dalton Trans.* **2008**, 2422. (f) Miyasaka, H.; Takayama, K.; Saitoh, A.; Furukawa, S.; Yamashita, M.; Clérac, R. *Chem.—Eur. J.* **2010**, *16*, 3656.

(40) Boča, R. *Coord. Chem. Rev.* **2004**, *248*, 757.

(41) Zhang, D.; Wang, H.; Tian, L.; Kou, H.-Z.; Jiang, J.; Ni, Z.-H. *Cryst. Growth Des.* **2009**, *9*, 3989.

(42) Miyasaka, H.; Matsumoto, H. I. N.; Re, N.; Crescenzi, R.; Floriani, C. *Inorg. Chem.* **1998**, *37*, 255.